

PREPARED FOR SUBMISSION TO JCAP

Big Bang Nucleosynthesis constraints on sterile neutrino and lepton asymmetry of the Universe

Graciela B. Gelmini,^a Masahiro Kawasaki,^{b,c} Alexander
Kusenko,^{a,c} Kai Murai,^{b,c} Volodymyr Takhistov^a

^aDepartment of Physics and Astronomy, University of California, Los Angeles, CA 90095-1547, USA

^bInstitute for Cosmic Ray Research, The University of Tokyo, Kashiwa 277-8582, Japan

^cKavli Institute for the Physics and Mathematics of the Universe (WPI), The University of Tokyo, Kashiwa 277-8583, Japan

E-mail: kawasaki@icrr.u-tokyo.ac.jp, kmurai@icrr.u-tokyo.ac.jp

Abstract. We consider the cosmological effects of sterile neutrinos with the masses of 150 – 450 MeV. The decay of sterile neutrinos changes the thermal history of the Universe and affects the energy density of radiation at recombination and the big bang nucleosynthesis (BBN) results. We derive severe constraints on the parameters of sterile neutrinos from the primordial abundances of helium-4 and deuterium. We also find that in a particular model the constraints can be considerably relaxed by assuming a large lepton asymmetry in the active neutrinos. In this case, the consistent parameters result in $N_{\text{eff}} \simeq 3.2 - 3.4$ and can alleviate the Hubble tension.

Keywords: sterile neutrino, big bang nucleosynthesis

Contents

1	Introduction	2
2	Sterile neutrinos in the early Universe	3
2.1	Production and decoupling	3
2.2	Energy density of the non-relativistic sterile neutrino	4
3	Sterile neutrino decay	6
3.1	Scattering of the high-energy neutrinos from the decay	7
3.2	Entropy generation and dilution effect	8
3.3	Change of N_{eff}	9
4	BBN and constraint on the sterile neutrino	10
4.1	Qualitative impact of the sterile neutrino	10
4.2	Observational constraints on the light elements	11
4.3	Constraints from BBN	11
5	BBN with lepton asymmetries	12
6	Discussion	14
A	Decay channels of sterile neutrino	17
A.1	$\nu_s \rightarrow 3\nu$	17
A.2	$\nu_s \rightarrow \nu_e + e^+ + e^-$	18
A.3	$\nu_s \rightarrow \nu_e + \mu^- + \mu^+$	18
A.4	$\nu_s \rightarrow e^- + \nu_\mu + \mu^+$	18
A.5	$\nu_s \rightarrow \nu_e + \pi^0$	18
A.6	$\nu_s \rightarrow e^- + \pi^+$	19
A.7	$\nu_s \rightarrow \nu_e + \gamma$	19
B	Annihilation of high-energy neutrinos from the decay	19
B.1	Lorentz transformation of cross sections	20
B.2	Annihilation of the decay products with the background neutrinos	20
B.3	Annihilation of the decay products with themselves	23
C	BBN results in more detail	24
D	Generation of a large lepton asymmetry	24

1 Introduction

The discovery of neutrino oscillations [1] has firmly established the existence of neutrino masses and flavor mixing. As weakly interacting (active) neutrinos are massless within the Standard Model (SM), this motivates new physics in the neutrino sector. While precision measurements of Z-boson decays restrict the number of active neutrino species to three [2], this does not exclude the presence of additional sterile neutrinos that are singlets under the SM gauge groups.

Sterile neutrinos have been extensively discussed in the literature, as they are motivated by various theoretical considerations and play a central role in models for the origin of the neutrino masses. In particular, they are essential for the seesaw mechanism [3–6], which utilizes sterile neutrinos much heavier than the electroweak scale to generate small masses for active neutrinos. While the three-flavor neutrino paradigm has been extensively tested, a slew of anomalous results consistent with the existence of additional sterile neutrino species of $m_s \sim \mathcal{O}(\text{eV})$ mass have been reported, including from MiniBooNE [7] and LSND [8] short baseline experiments, gallium experiments [9, 10], measurements of reactor neutrino flux [11] as well as combined fits [12–14] to data from NEOS [15] and DANSS [16] reactor experiments. Sterile neutrinos with mass of $m_s \sim \mathcal{O}(\text{keV})$ have been investigated in the context of dark matter [17–33]. Furthermore, keV sterile neutrinos can also play a role in supernova explosions [34–36] and in generating the matter-antimatter asymmetry of the universe [23, 37–39]. For an overview of sterile neutrinos see, e.g., Ref. [40].

While sterile neutrinos with sub-MeV mass have already garnished significant consideration, heavier sterile neutrinos have not been as well explored. Heavy sterile neutrinos with mass $m_s \lesssim \text{GeV}$ that mix with active neutrinos with strength below the current laboratory bounds and decaying around the time of Big Bang Nucleosynthesis (BBN) can affect the thermal history of the Universe in a profound manner. Previously, in Ref. [41], one of the present authors and collaborators derived the constraints on heavy sterile neutrino mass and mixing parameters from the Cosmic Microwave Background (CMB) limit on the effective number of relativistic neutrino species N_{eff} (see Ref. [42] for another possible effect on the CMB of sterile neutrinos in a similar mass range). However, it is also paramount to address constraints from BBN, as sterile neutrinos decaying around the BBN epoch can dramatically affect the abundances of the synthesized light elements (D and ^4He). The lifetime of heavy sterile neutrinos has been roughly restricted from above by BBN considerations [43] (see also Ref. [44]), but detailed analyses of BBN effects and constraints were only performed for sterile neutrinos lighter than the pion [45–48].

In this paper, we investigate the effect on BBN of heavy sterile neutrinos with the mass $150 \text{ MeV} < m_s < 450 \text{ MeV}$ that mix only with electron neutrinos and decay just after e^+e^- annihilation. Lighter sterile neutrinos, with $m_s < 150 \text{ MeV}$, are severely constrained by the CMB limit on N_{eff} [41]. For heavier ones, with $m_s > 450 \text{ MeV}$, one needs to include additional

decay channels of sterile neutrinos into kaons, eta, or 3 pions.

We find that BBN imposes stringent constraints on the allowed sterile neutrino parameter space. Further, we point out that the BBN limits can be relaxed if there is a large lepton asymmetry before the BBN epoch, and study this situation in a particular model.

This paper is organized as follows. In Sec. 2, we summarize the behavior of the sterile neutrinos in the early Universe. In Sec. 3, we review the decay of sterile neutrinos and its effects on cosmology. We give the results of the BBN calculations with the sterile neutrino in Sec. 4 and the results of a particular model with lepton asymmetries in Sec. 5. Finally, our conclusions and discussions are in Sec. 6.

2 Sterile neutrinos in the early Universe

The existence of the sterile neutrinos changes the cosmological scenario. In the following, we consider how the sterile neutrinos affect the thermal history of the Universe.

2.1 Production and decoupling

We assume that the sterile neutrinos are produced exclusively through their mixing with active neutrinos¹ while they are relativistic, i.e. when the cosmic temperature is

$$T > m_s . \quad (2.1)$$

First, we will check if sterile neutrinos were in thermal equilibrium at high temperatures. In this case, the production rate of the sterile neutrinos through their mixing with the electron neutrino should be larger than the cosmic expansion rate, the Hubble parameter H . Since the sterile neutrinos are produced through the weak interactions and the mixing, the production rate Γ_{prod} can be estimated by $\Gamma_{\text{prod}} \simeq G_F^2 T^5 \sin^2 \theta_M$, where G_F is the Fermi constant and θ_M is the active-sterile neutrino mixing angle in the medium. The mixing angle in the medium is related to the mixing angle in the vacuum θ as

$$\sin^2 \theta_M \sim \frac{\sin^2 \theta}{[1 + 9.6 \times 10^{-24} (T/\text{MeV})^6 (m_s/150\text{MeV})^{-2}]^2} , \quad (2.2)$$

in the limit of small mixing [49]. Thus, matter effects become important when

$$T \gtrsim 6.9 \text{ GeV} \left(\frac{m_s}{150\text{MeV}} \right)^{1/3} . \quad (2.3)$$

Therefore, the condition for sterile neutrinos to be in thermal equilibrium is

$$\frac{\Gamma_{\text{prod}}}{H} \simeq \frac{G_F^2 T^5 \sin^2 \theta_M}{\sqrt{\frac{\pi^2 g_*}{90}} \frac{T^2}{M_{\text{Pl}}}} > 1 . \quad (2.4)$$

¹We note that sterile neutrinos could also be produced through other mechanisms beyond active-sterile neutrino mixing, such as decays of additional heavy scalars in non-minimal particle models [25, 26].

Here $M_{\text{Pl}} \simeq 2.4 \times 10^{18}$ GeV is the (reduced) Planck mass. By rewriting this as a condition for the temperature, we obtain

$$T \gtrsim \left(\frac{\pi^2 g_*}{90} \right)^{1/6} G_F^{-2/3} M_{\text{Pl}}^{-1/3} \left(\frac{1}{\sin^2 \theta_M} \right)^{1/3} \simeq 4.5 \text{ GeV} \left(\frac{g_*}{86.25} \right)^{1/6} \left(\frac{10^{-10}}{\sin^2 \theta_M} \right)^{1/3} = T_{\text{f.o.}}, \quad (2.5)$$

where we take $g_* = 86.25$ as a reference value for the number of degrees of freedom in the thermal bath that corresponds to $m_b < T < m_W$, where $m_b = 4.2$ GeV is the mass of the bottom quark and $m_W = 80.4$ GeV is the mass of the W gauge boson. If the condition in Eq. (2.4) is satisfied at high temperatures $T > T_{\text{f.o.}}$, then $T_{\text{f.o.}}$ is the decoupling or freeze-out temperature. As we can see from Eq. (2.5), sterile neutrinos are already decoupled at $T \sim m_b$ for $\sin^2 \theta < 10^{-10}$, because $\sin^2 \theta_M < \sin^2 \theta$. Therefore, the value $g_* = 86.25$ is justified for $\sin^2 \theta < 10^{-10}$. By comparing Eqs. (2.3) and (2.5), we find that sterile neutrinos are thermally produced and the matter effects are negligible if $\sin^2 \theta \gtrsim 2.8 \times 10^{-11} (m_s/150 \text{ MeV})^{-1}$.

On the other hand, for a smaller mixing, matter effects become important and sterile neutrinos may not be thermally produced. In this case, sterile neutrinos are non-thermally produced through active-sterile neutrino oscillations, which is known as the Dodelson-Widrow (DW) mechanism [17]. The produced sterile neutrinos are less abundant than those produced thermally and experience entropy dilution after their production, which happens mostly at a temperature T_{max} at which the DW production rate is maximum. However, these sterile neutrinos can still affect the BBN and thus can be constrained by BBN. Considering the entropy dilution after T_{max} , the number density at $T \sim 1$ MeV of non-thermally produced sterile neutrinos at $T \sim 1$ MeV can be written as [49, 50]

$$n_{\nu_s}(T) = \left(1 - \exp \left[-3.27 \left(\frac{\sin^2 \theta}{10^{-10}} \right) \left(\frac{m_s}{150 \text{ MeV}} \right) \right] \right) \frac{g_{s*}(T)}{g_{s*,\text{prod}}} n_{\nu_\alpha}(T) \quad (2.6)$$

where n_{ν_α} is the number density of one active neutrino species and $g_{s*,\text{prod}} = 86.25$ is the number of relativistic degrees of freedom when sterile neutrinos are produced. The DW production rate is maximum at $T_{\text{max}} \simeq 5.7 \text{ GeV} (m_s/150 \text{ MeV})^{1/3}$, when $\sin \theta_M / \sin \theta = 1/1.34$ [51]. We can consider that sterile neutrinos are mainly produced at T_{max} and use $g_{s*,\text{prod}} = 86.25$ for our purpose. From the BBN upper bound of $N_{\text{eff}} < 3.4$ [52] (see also Particle Data Group [53]), we can conclude that sterile neutrinos are constrained by BBN when $\rho_{\nu_s} = m_s n_{\nu_s} > 0.4 \rho_{\nu_\alpha}$ at BBN ($T \sim 1$ MeV). Using Eq. (2.6) when the exponent is small, this condition implies

$$\sin^2 \theta > 2.0 \times 10^{-12} \left(\frac{m_s}{150 \text{ MeV}} \right)^{-2}. \quad (2.7)$$

2.2 Energy density of the non-relativistic sterile neutrino

We now calculate the energy density of the sterile neutrinos before they decay. Here, we focus on the sterile neutrinos that decay at temperatures lower than the MeV scale. As we show in detail in Sec. 3.1 and Appendix B, in this case the re-scattering of active neutrinos

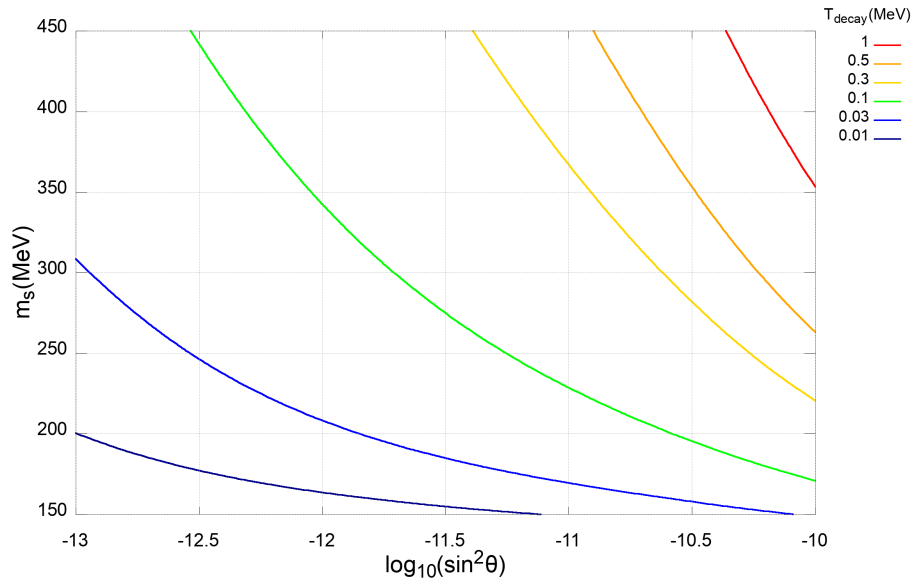


Figure 1: Temperature of the Universe when the sterile neutrinos decay. Note that, since we assume the decay occurs after the electron-positron annihilation we consider only the region in which $T_{\text{decay}} < 0.5$ MeV.

produced in the decay is negligible. Thus, sterile neutrinos with mass $m_s > 150$ MeV behave like matter when they decay.

The energy density of non-relativistic sterile neutrinos ρ_{ν_s} when they decay is

$$\rho_{\nu_s}(T_{\text{decay}}) = m_s n_{\nu_s}(T_{\text{decay}}), \quad (2.8)$$

where T_{decay} is the cosmic temperature when sterile neutrinos decay.

The non-relativistic sterile neutrinos can dominate the Universe before they decay, when

$$\Gamma_{\text{decay}} = H(T), \quad (2.9)$$

where the Hubble parameter is

$$H(T) = \sqrt{\frac{\rho_{\nu_s} + \rho_R}{3M_{\text{Pl}}^2}} = \frac{1}{\sqrt{3}M_{\text{Pl}}} \left[m_s n_{\nu_s}(T) + g_*(T) \frac{\pi^2}{30} T^4 \right]^{\frac{1}{2}}. \quad (2.10)$$

Considering only sterile neutrinos that decay after the electron-positron annihilation, and thus $g_{s^*}(T_{\text{decay}}) = 43/11$ and $g_*(T_{\text{decay}}) = 2 + (21/4)(4/11)^{4/3}$, the decay temperature is shown in Fig. 1. In the following, we focus on the regions where $T_{\text{decay}} < m_e \simeq 0.5$ MeV.

Using T_{decay} , we calculate the energy ratio of sterile neutrinos and radiation at decay. The results, plotted in Fig. 2, show that the Universe could have been dominated by the non-relativistic sterile neutrinos just before they decayed.

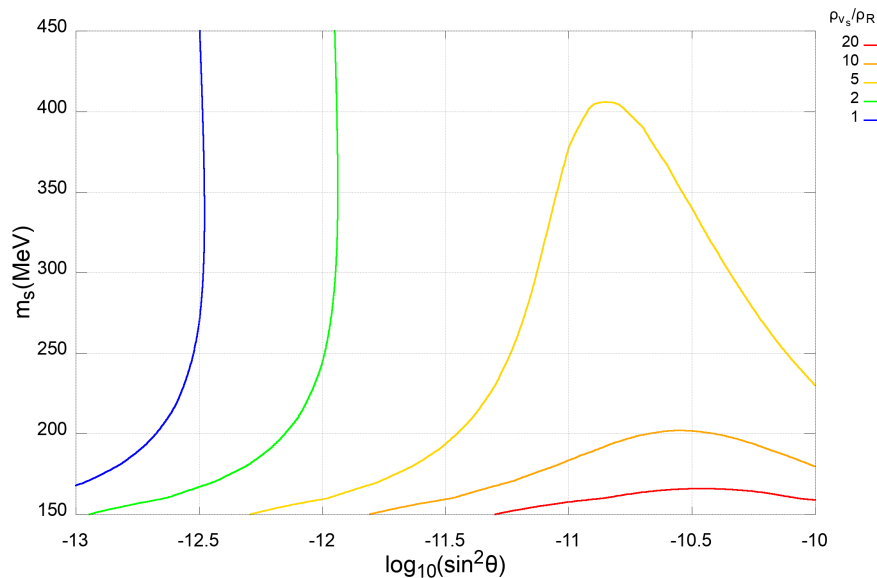


Figure 2: Ratio of sterile neutrino and radiation energy densities when the sterile neutrinos decay.

3 Sterile neutrino decay

As mentioned above, heavy sterile neutrinos decay after the decoupling of active neutrinos. Since the sterile neutrinos inject their energy into both the plasma and the neutrino sector through their decays, these cause entropy production and change N_{eff} .

The decay channels we consider are summarized in App. A. For each channel, the decay rate Γ and the energy fraction f injected into the plasma are also shown in App. A. Using them for each channel, the total sterile neutrino decay rate and the average \bar{f} can be obtained. The decay channels in Appendix A are all the processes where a sterile neutrino produces an electron neutrino through their mixing. Therefore, the decay rates are all proportional to $\sin^2\theta$ and the branching ratios depend only on m_s . We show the branching ratios in Fig. 3 (a) and \bar{f} in Fig. 3 (b). Here, we assume that the sterile neutrinos decay after active neutrino decoupling and the neutrinos produced in the decay do not inject energy into the plasma sector. Although the neutrinos with high energy do inject some fraction of their energy into the plasma through annihilations or scatterings or modify the neutron-proton ratio through weak interaction [45], as we discuss in Sec. 3.1, we will restrict ourselves to the regions in the mass and mixing parameter space where these effects are negligible.

The sterile neutrino lifetime is shown in Fig. 4. As we can see from the decay rate for each channel in App. A, the heavier the sterile neutrino is and the larger the mixing angle is, the shorter is the lifetime.

We note that, in contrast to Ref. [41], in our study we employ the more detailed calcu-

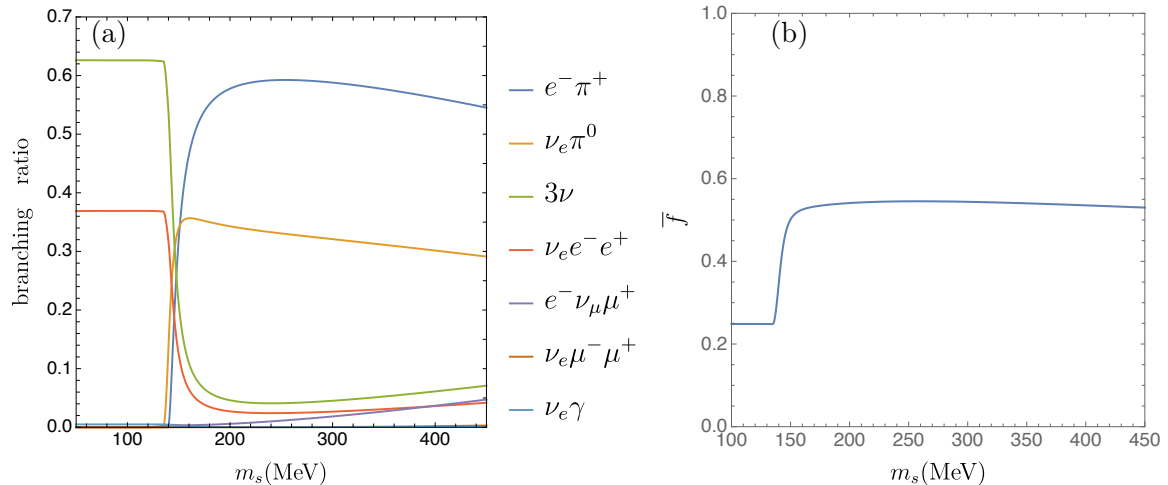


Figure 3: (a) Branching ratios of the sterile neutrino decay modes. They depend only on m_s (and not on $\sin\theta$). (b) The average fraction \bar{f} of the sterile neutrino rest mass injected into the plasma.

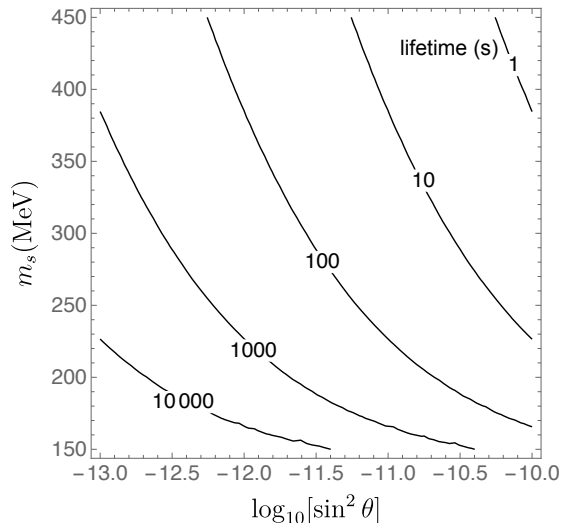


Figure 4: The sterile neutrino lifetime.

lations of Ref. [54] for the rates of the relevant sterile neutrino decay channels. The resulting entropy generation, dilution and change in effective number of relativistic neutrino species N_{eff} from our analysis are qualitatively in agreement with those of Ref. [41].

3.1 Scattering of the high-energy neutrinos from the decay

In the estimation of the average fraction \bar{f} above, we assumed the neutrinos produced in the decay do not inject any energy into the thermal plasma sector. Here we comment on a possible correction to \bar{f} due to the interaction of the high energy neutrinos. Since active neutrinos can

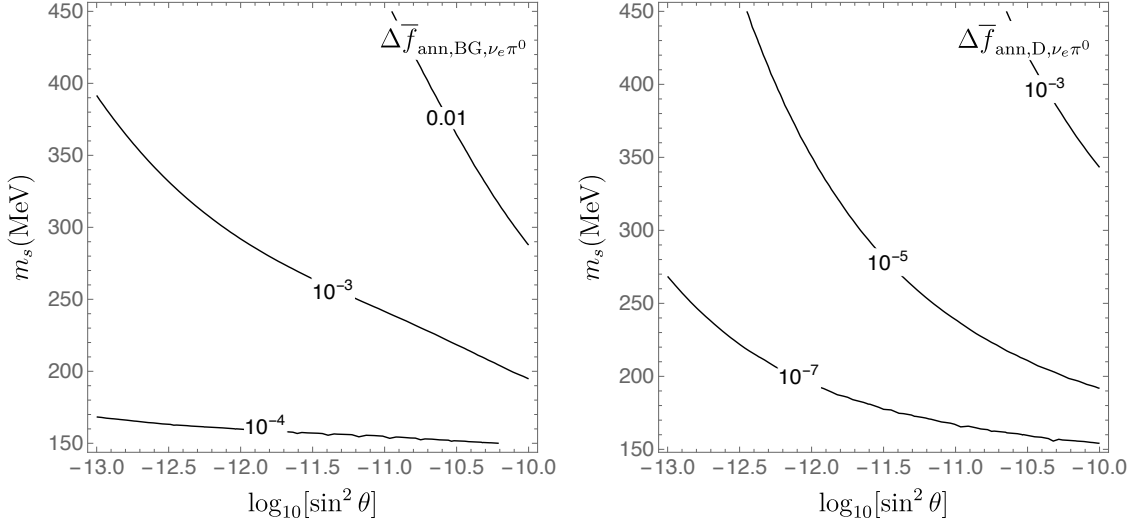


Figure 5: The correction to \bar{f} due to the annihilation of the high-energy neutrinos produced from $\nu_s \rightarrow \nu_e + \pi^0$ process. The left panel shows the correction from the annihilation of the high-energy neutrinos and the background neutrinos. The right panel shows the correction from the annihilation of the high-energy neutrinos themselves.

produce electrons and positrons through weak interactions with other particles in the thermal bath, we can consider two situations:

- The active neutrinos produced in the decay interact with the background particles.
- The active neutrinos produced in the decay interact with each other.

For each situation, we focus on the $\nu_s \rightarrow \nu_e + \pi^0$ decay process that is the dominant decay mode and estimate the correction to \bar{f} due to the annihilation process $\nu_e + \bar{\nu}_e \rightarrow e^- + e^+$, shown in Fig.5. From the figure it is seen that the correction is smaller than 0.01 in most of the parameter space and it is larger for scatterings off the background neutrinos. In the following we only consider the parameter region satisfying $\Delta\bar{f}_{\text{ann,BG},\nu_e\pi^0} < 0.01$ in the left panel of Fig.5 and hence neglect the correction. For a detailed discussion see App. B.

For the parameter region where \bar{f} receives negligible corrections, the weak interaction processes involving high-energy neutrinos are also negligible and the modification of the neutron-proton ratio can be ignored.

3.2 Entropy generation and dilution effect

The sterile neutrinos inject their energy into the plasma sector and the neutrino sector through their decay and generate entropy. Here we define the ratio F of the entropy after (s_f) and before (s_i) the decay

$$F \equiv \frac{s_f}{s_i} = \frac{g_f T_f^3 a_f^3}{g_i T_i^3 a_i^3}. \quad (3.1)$$

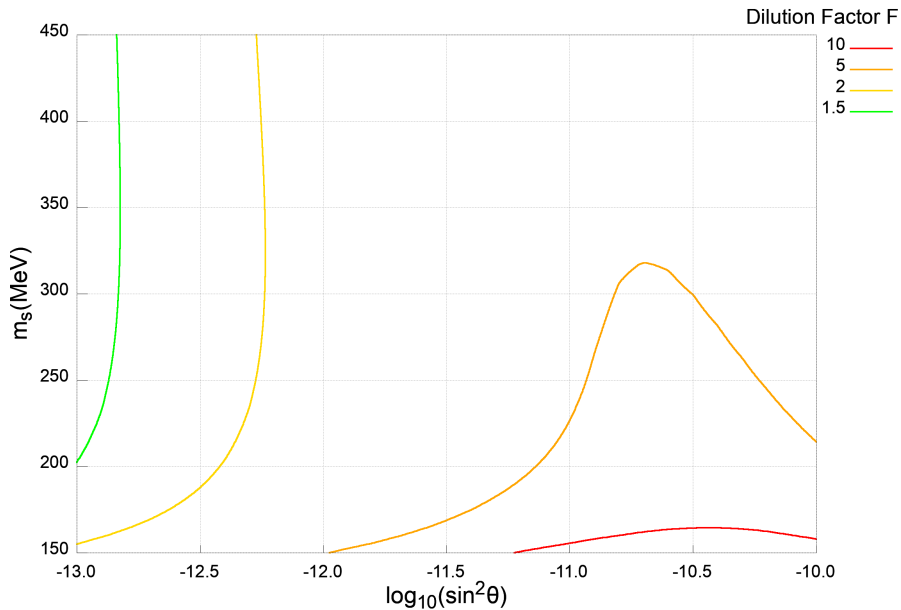


Figure 6: Ratio F of the entropies after and before the sterile neutrino decay.

The subscript i indicates the time before the sterile neutrinos begin to decay and the subscript f indicates the time after most of the sterile neutrinos decayed. We take the number of degrees of freedom of the plasma to be $g_i = 11/2$ and $g_f = 2$. In other words, the decays occur after active neutrino decoupling and finish after the electron-positron annihilation. Using F , we can compute the ratio of the photon and neutrino temperatures after the decay. Since T_ν satisfies $T_\nu a_f = T_{\nu i} a_i$,

$$\frac{T_{\nu f}}{T_f} = \frac{a_i}{a_f} \cdot \frac{T_i}{T_f} = \frac{1}{F^{1/3}} \left(\frac{g_f}{g_i} \right)^{1/3} = \frac{1}{F^{1/3}} \left(\frac{4}{11} \right)^{1/3}, \quad (3.2)$$

where we used $T_{\nu i} = T_i$.

This entropy generation has a significant impact on BBN. Considering it and the value of $\eta \equiv n_B/n_\gamma$ inferred from CMB observations, we can conclude that η has a higher value in the BBN epoch than in the standard scenario. We show entropy ratio F values in the $(\sin^2 \theta, m_s)$ plane in Fig. 6.

3.3 Change of N_{eff}

The decay of the sterile neutrino changes the effective number of neutrino species N_{eff} , which is defined through the relation

$$\rho_R = \left(1 + \frac{7}{8} \left(\frac{4}{11} \right)^{4/3} N_{\text{eff}} \right) \rho_\gamma, \quad (3.3)$$

where ρ_R is the total radiation energy density including the background and neutrinos produced due to the decays, and ρ_γ is the photon energy density. In our scenario, the decay of

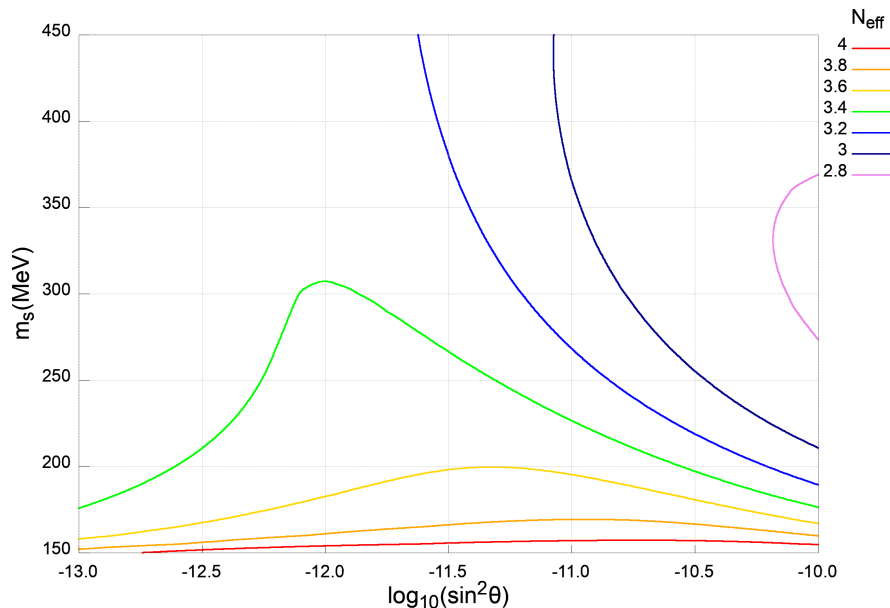


Figure 7: N_{eff} after the sterile neutrino decay.

the sterile neutrinos injects some energy into the plasma and the neutrino sector. Therefore, N_{eff} after the decay largely depends on the energy injection ratio \bar{f} .

In Fig. 7 we show N_{eff} after the decay of the sterile neutrinos. Our results confirm the observation of Ref. [41] that N_{eff} can take values close to 3 in some region of the parameter space.

4 BBN and constraint on the sterile neutrino

In this section, we show that the sterile neutrino parameters are tightly constrained by BBN considerations. Following the usual BBN conventions, we write the abundances of the primordial ${}^4\text{He}$ and D as Y_p and D/H. Y_p is defined as the ratio of the ${}^4\text{He}$ mass density and the total baryon density ($= \rho_{{}^4\text{He}}/\rho_B$) while D/H is the ratio of the D and H number densities ($= n_D/n_H$).

4.1 Qualitative impact of the sterile neutrino

First, we discuss qualitatively the effects of the sterile neutrinos on BBN. The sterile neutrinos have a significant energy density before they decay, which increases the cosmic expansion faster. The faster cosmic expansion during BBN results in an earlier freeze-out of the weak interactions and a larger neutron-to-proton ratio. This speed-up effect makes D/H and Y_p larger.

As mentioned in Sec. 3.2, the entropy generation by the sterile neutrino decay means a larger η during the BBN epoch. This effect makes D/H smaller and Y_p larger. However, if

the sterile neutrinos decay before the synthesis of D ($T \simeq 0.1$ MeV), the entropy generation does not significantly affect BBN.

4.2 Observational constraints on the light elements

Here we summarize observational constraints on the primordial abundances of D and ^4He . The deuterium abundance has been precisely determined by observing absorption spectra of QSOs due to damped Lyman- α systems. Recently, Cooke *et al.* [55] reported

$$(\text{D}/\text{H})_p = (2.527 \pm 0.030) \times 10^{-5}, \quad (4.1)$$

from measurements of the 7 damped Lyman- α systems. This estimation is consistent with $(\text{D}/\text{H})_p = (2.545 \pm 0.025) \times 10^{-5}$ obtained by Zavaryzin *et al.* [56]. The Particle Data Group [53] suggests $(\text{D}/\text{H})_p = (2.547 \pm 0.025) \times 10^{-5}$ which is almost the same as that given in [56].

The primordial abundance of ^4He is determined by measurements of recombination lines from extra-galactic HII regions. Izotov *et al.* [57] obtained $Y_p = 0.2551 \pm 0.0022$ from the observation of 45 extragalactic HII regions. However, Aver, Olive and Skillman [58] reanalyzed the data of Ref. [57] and obtained $Y_p = 0.2449 \pm 0.0040$. These two measurements are inconsistent with each other. Since more recent measurements [59, 60] are in good agreement with result the of Ref. [58], in this paper we adopt the value obtained by Aver, Olive and Skillman [58],

$$Y_p = 0.2449 \pm 0.0040. \quad (4.2)$$

On the other hand, the Particle Data Group [53] adopts the more stringent constraint $Y_p = 0.245 \pm 0.003$.

As for the baryon-to-photon ratio η_B we adopt

$$\eta_B = (6.138 \pm 0.038) \times 10^{-10}, \quad (4.3)$$

from Planck observations [61].

4.3 Constraints from BBN

We show the result of our BBN numerical calculations in Fig. 8. We modified the public BBN code `PArthENoPE2.0` [62, 63] for our purpose. In our calculations, the baryon density after the BBN epoch is fixed by the estimation of Planck 2018 [61]. For the uncertainties of D/H and Y_p , we included the uncertainties of the `PArthENoPE2.0` calculation, the baryon density of Planck 2018, and the observational estimations. Fig. 8 shows the region where the numerical calculations and the observational estimates match at the 68% and 95% confidence levels. As observational estimates we used Cooke *et al.* [55] for D/H and Aver *et al.* [58] for Y_p . In the gray shaded region our estimation for f would require non-negligible corrections, as discussed in Sec. 3.1, and we do not consider this parameter region in this paper.

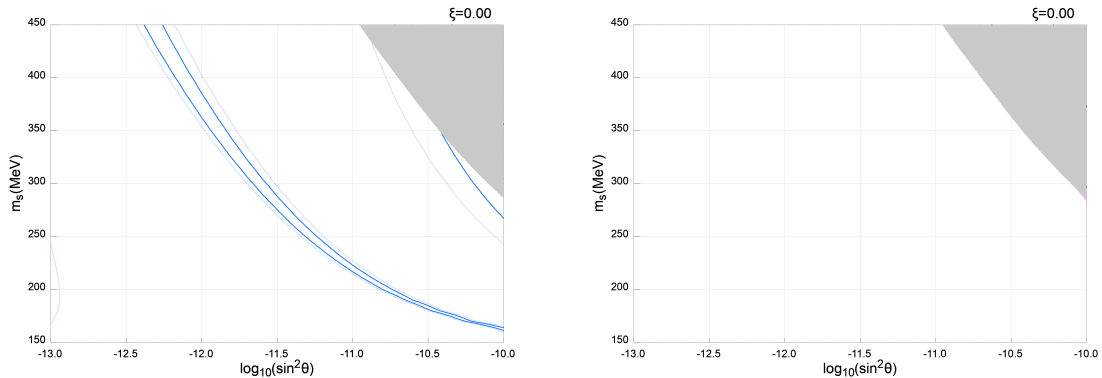


Figure 8: Regions of agreement of our numerical calculations of BBN with sterile neutrinos and data. In the left panel, dark and light blue lines indicate the boundaries of the regions allowed at the 68% and 95% C.L. by D/H data, respectively. No regions allowed by Y_P limits were found. The right panel shows the results of the combined analysis of D/H and Y_P . There are no allowed regions in the combined analysis. Our calculations are not valid in the gray shaded region. All the un-shaded region is thus inconsistent with the BBN data at the 95% C.L.

As mentioned before, both the Hubble expansion speed-up effect and entropy production by the sterile neutrinos increases ${}^4\text{He}$. Thus, ${}^4\text{He}$ is overproduced unless the sterile neutrinos decay before BBN starts. On the other hand, the increase of the D abundance by the speed-up effect can be compensated by its decrease due to entropy production, which yields the narrow allowed region between blue lines for D in Fig. 8, which is consistent with the previous constraint given in Ref. [44]. As a result, there is no region which satisfies the observational constraints on both ${}^4\text{He}$ and D in the unshaded region in Fig. 8. Therefore, we conclude that the unshaded region in Fig. 8 is inconsistent with the BBN data at the 95% C.L. This is a more severe constraint than that from N_{eff} .

5 BBN with lepton asymmetries

In the previous section we have seen that the sterile neutrinos we considered are almost ruled out by the overproduction of ${}^4\text{He}$. However, the BBN constraint can be alleviated if some effect decreases the ${}^4\text{He}$ abundance. At the freeze-out of the weak interactions, the neutron-proton ratio in chemical equilibrium is given by

$$\left. \frac{n_n}{n_p} \right|_{\text{eq}} \simeq \exp \left[-\frac{m_n - m_p + \mu_{\nu_e}}{T} \right], \quad (5.1)$$

where μ_e is the chemical potential of the electron neutrinos with momentum distribution function $f(p) = [\exp((p - \mu_e)/T) + 1]^{-1}$. Therefore, a positive μ_{ν_e} reduces the neutron-proton ratio at the freeze-out and can cancel the effect of the Hubble expansion speed-up by

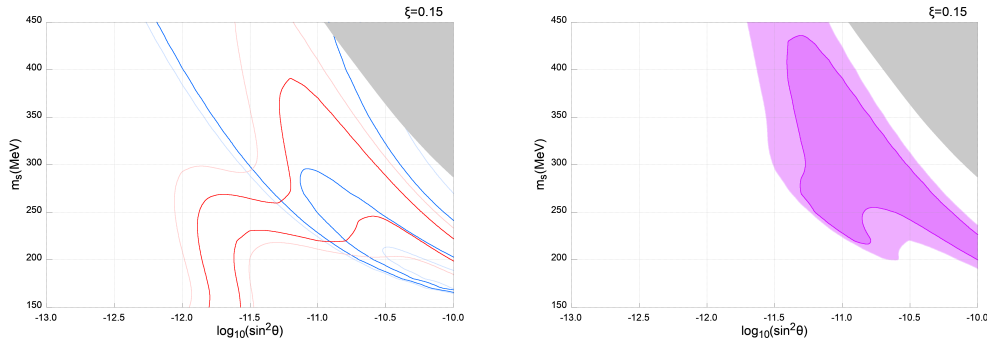


Figure 9: Results of our numerical calculation of BBN with sterile neutrinos and a lepton asymmetry with $\xi = 0.15$. In the left panel, dark and light blue lines indicate the boundaries of the regions of compatibility at the 68% and 95% C.L. for D/H, respectively and dark and light red lines indicate the same for Y_P . In the right panel, dark and light purple indicate regions allowed at the 68% and 95% C.L. by the combined analysis of D/H and Y_P .

the sterile neutrinos. In the following, we assume that the three active neutrinos have the same chemical potential μ and consider the effect of a large $\xi \equiv \mu/T_\nu$ on BBN.

A large ξ implies that there exists a large lepton asymmetry of the Universe. We assume that the lepton asymmetry is generated after sterile neutrinos decouple (if they reach thermal equilibrium) or are produced via active sterile oscillations and with a negligible accompanying entropy production, as explained in App. D. With these assumptions the large lepton asymmetry does not affect the production of the sterile neutrinos or the subsequent evolution of its number density. Since charge neutrality requires that the number of charged leptons and anti-leptons should be equal to the baryon asymmetry, the large lepton asymmetry we assume is carried by the three active neutrinos. The lepton asymmetry η_L , the ratio of the lepton number density to the entropy density, is

$$\eta_L = \frac{n_L}{s} = \frac{1}{s} \sum_{i=e,\mu\tau} (n_{\nu_i} - n_{\bar{\nu}_i}) = 0.106 \xi . \quad (5.2)$$

Here s is the entropy density before the entropy production by the sterile neutrino decays.

The results of the numerical calculations with $\xi = 0.15$ are shown in Fig. 9. Results with other values of ξ and comments on the choice of observational constraints are given in App. C. For $\xi \simeq 0.15$, $N_{\text{eff}} \simeq 3.2 - 3.4$ can be realized while maintaining the consistency of D/H and Y_P as shown in Fig. 10. This value of N_{eff} can alleviate the Hubble tension between CMB observations and direct measurements [64].

The $N_{\text{eff}} \simeq 3.0 - 3.4$ range allowed in our BBN analysis for $\xi \simeq \mathcal{O}(0.1)$ is consistent with current constraints imposed on the (N_{eff}, ξ) plane by CMB and other observations [65–67]. Note that our scenario predicts that the value of ξ relevant for CMB observations, call it ξ_{CMB} , is actually the ξ we used divided by F , i.e. $\xi_{\text{CMB}} = \xi/F$, because the entropy generation due to the sterile neutrinos decay also dilutes the lepton asymmetry. In Fig. 11, we show lines

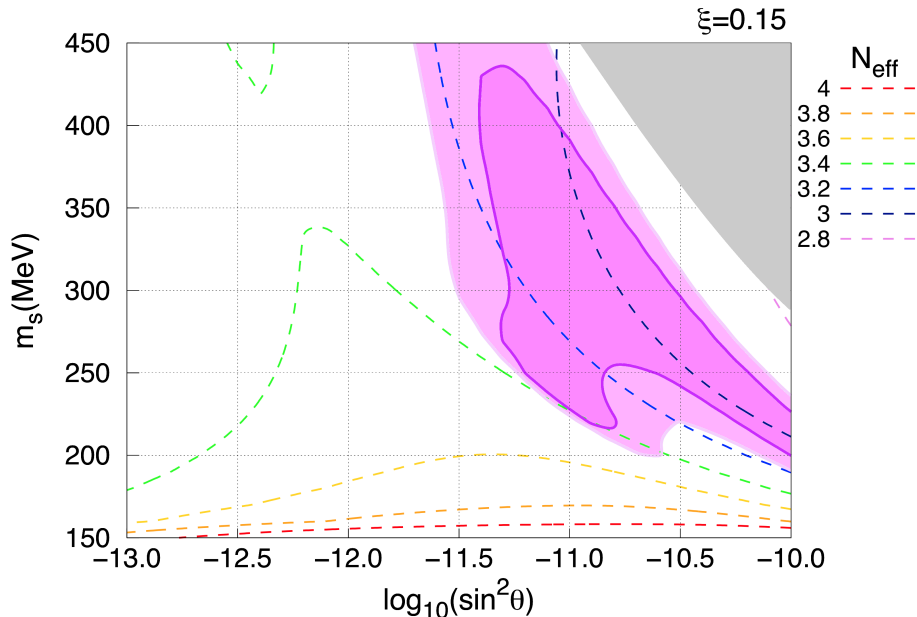


Figure 10: N_{eff} values and regions allowed by our BBN results with $\xi = 0.15$ (as in the right panel of Fig. 9). The allowed region includes the range $N_{\text{eff}} \simeq 3.2 - 3.4$, which can alleviate the tension between local and early Universe measurements of the Hubble constant [64].

of constant entropy ratio F and the BBN allowed region for $\xi = 0.15$. We can see that the region consistent with BBN indicates that $F \simeq 5$.

In Fig. 12 we display the regions of mass and mixing inconsistent with the BBN data, with and without lepton asymmetry, as well as the current laboratory constraints on a heavy sterile neutrino that mixes with the electron neutrino.

6 Discussion

In this work, we investigated the impact on BBN of heavy sterile neutrinos with the mass range $150 \text{ MeV} < m_s < 450 \text{ MeV}$ that decay after electron-positron annihilation. We find that BBN severely constrains the sterile neutrino mass m_s and active-sterile mixing $\sin \theta$ parameter space. The obtained constraints are significantly more stringent than those obtained from limits on N_{eff} .

We found that the constraints from BBN can be drastically relaxed by the introduction of a large lepton asymmetry $\xi \sim \mathcal{O}(0.1)^2$, assuming the large lepton asymmetry is accounted for

²During the preparation of this manuscript, a paper on a related topic was released [76]. This paper suggests that the combination of entropy generation, extra radiation energy, and lepton asymmetries can be consistent with BBN. Our work confirms this suggestion by calculating BBN in a specific situation.

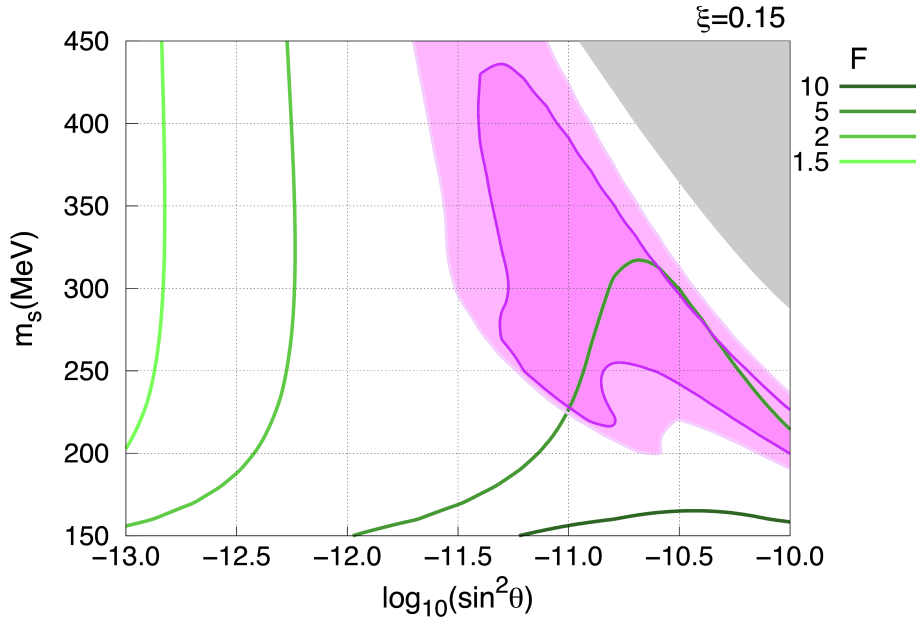


Figure 11: Ratio F of the entropy after and before the sterile neutrino decays and the region allowed by our BBN results with $\xi = 0.15$ (as in the right panel of Fig. 9). In this region $F \simeq 5$.

independently of the sterile neutrino production. Notice that such a large lepton asymmetry should be produced at sufficiently late times. If a large lepton asymmetry is produced in the early Universe at $T > 100$ GeV, sphaleron processes convert a significant fraction of the lepton number to baryon number, which leads to a too large baryon asymmetry $\eta_B \gg 10^{-9}$ of the present Universe. In order to produce a large lepton asymmetry with $\xi \sim \mathcal{O}(0.1)$, a special setup is required, for example if Q-balls that contain lepton charges form in the early Universe and decay after the electroweak phase transition.

For simplicity, we assumed that the large lepton asymmetry is generated at $T < \text{few GeV}$, after the decoupling (if they reached thermal equilibrium) or production (via active-sterile oscillations) of sterile neutrinos, thus these processes are not affected by it, as mentioned in App. 5. Moreover, as explained in App. D, the entropy production associated with the generation of the large lepton number asymmetry via Q-balls decay (which is model-dependent) could be negligible, as we assume here. With these assumptions the production and evolution of the sterile neutrino number density is the same as without the large lepton density.

With a large lepton asymmetry $\xi \sim \mathcal{O}(0.1)$, BBN limits allow the $N_{\text{eff}} \simeq 3.2 - 3.4$ range, that could alleviate the tension between local and early Universe measurements of the Hubble constant. The values of N_{eff} and ξ allowed by our BBN analysis are consistent with CMB

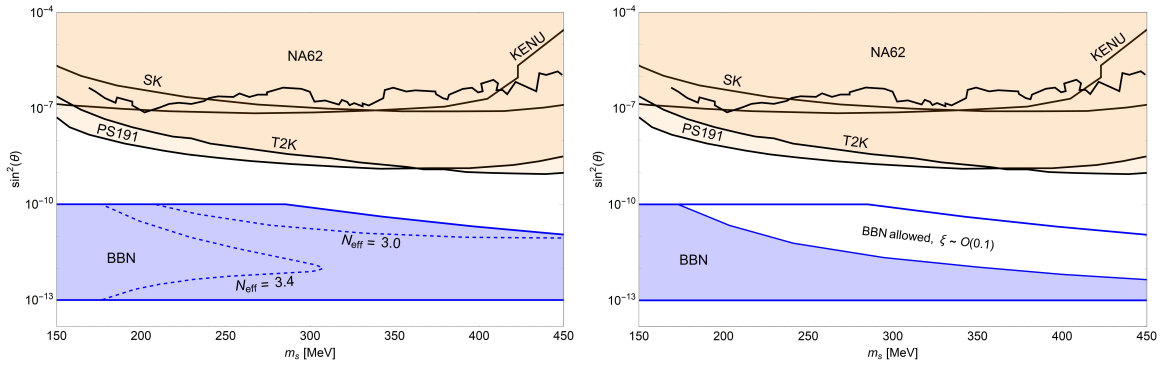


Figure 12: Regions inconsistent with the BBN data (blue) of heavy sterile neutrinos mixing with electron neutrinos for zero lepton asymmetry [left panel] and large lepton asymmetry with $\xi = \mathcal{O}(0.1)$ [right panel], along with regions (orange) rejected by existing upper bounds from the T2K near detector [68], NA62 [69], PS191 [70, 71], Super-Kamiokande (labeled “SK”) - as derived in Ref. [72, 73], and precision measurements of kaon decays (labeled “KENU”) [74] as derived in Ref. [75]. The (dark blue) upper boundary of the region in which our BBN results apply corresponds to $\sin^2(\theta) = 10^{-10}$ and to the lower boundary of the gray region shown in previous figures, excluded from our analysis (because the energy fraction f injected into the plasma would receive non-negligible corrections as, discussed in text). The (dark blue) lower boundary is set by the reach of our numerical calculations, $\sin^2(\theta) = 10^{-13}$. The lines of $N_{\text{eff}} = 3.0$ and $N_{\text{eff}} = 3.4$ for no lepton asymmetry are indicated (dashed blue lines) in the left panel. The right panel shows that a sizable lepton asymmetry, $\xi = \mathcal{O}(0.1)$, allows to remove BBN constraints in the part of the region where $N_{\text{eff}} = 3.0 - 3.4$, which is consistent with CMB observations and alleviates the Hubble constant tension.

limits. The relaxation of the BBN limits on N_{eff} with $\xi \sim \mathcal{O}(0.1)$ is shown in Fig. 12, where we display the regions of mass and mixing inconsistent with the BBN data with and without a lepton asymmetry, as well as current laboratory upper bounds on the mixing, assuming that the sterile neutrino only mixes with the electron neutrino (as we do in this work).

The cosmological effects of heavy decaying sterile neutrinos go beyond just BBN. Non-thermal active neutrinos with high energy produced in the decay of the sterile neutrinos have a larger free-streaming length than the thermal neutrinos in the standard scenario. Therefore, the decay of the sterile neutrinos induces a suppression of the matter power spectrum at large scales (see e.g. Ref. [77]). Furthermore, while we have concentrated on phenomenological aspects related to BBN, as already noted in Ref. [41], heavy decaying sterile neutrinos provide an interesting setting for model-building. In particular, the significant entropy dilution due to the sterile neutrino decays can allow light decoupled particles to avoid cosmological bounds, and the change in the baryon-to-entropy ratio it produces affects models of baryogenesis.

The parameter region studied in this work is restricted by some assumptions and the reach of our numerical calculations. By expanding the explored regions, we may be able to impose more severe constraints on sterile neutrinos or find more extended allowed regions,

which will be done in future work.

Acknowledgments

M. Kawasaki is grateful to the Department of Physics and Astronomy, University of California, Los Angeles for hospitality during the time when this work started. This work was supported by JSPS KAKENHI Grant Nos. 17H01131 (M.K.) and 17K05434 (M.K.), MEXT KAKENHI Grant Nos. 15H05889 (M.K.), World Premier International Research Center Initiative (WPI Initiative), MEXT, Japan (M. K. and K. M.), the Program of Excellence in Photon Science (K. M.), and the JSPS Research Fellowships for Young Scientists Grant No. 20J20248 (K. M.). The work of G.G., A.K and V.T. was supported by the U.S. Department of Energy (DOE) Grant No. DE-SC0009937.

A Decay channels of sterile neutrino

In the following we summarize the decay channels of a sterile neutrino with the mass of $150 \text{ MeV} \lesssim m_s \lesssim 450 \text{ MeV}$. Here we assume that the sterile neutrino mixes only with the electron neutrinos and show only the channels where the sterile neutrino changes into an electron neutrino. If the sterile neutrino is Majorana, each channel has its counterpart where the sterile neutrino changes into an anti-electron neutrino. In this paper, we assume that the sterile neutrino is Majorana and the decay rate is double the sum of the decay rates below. For each decay channel, we show the decay rate and the fraction of the sterile neutrino rest mass deposited in the thermal plasma f . In estimating f we assume that neutrinos in the final state do not interact with the other particles and do not give their energy to the thermal plasma. The justification of this assumption is examined in Appendix B. In the calculation, the physical constants were taken from [53]. The decay rates in Sec. A.1 to Sec. A.6 follow Ref. [54] and that in Sec. A.7 follows Ref. [20]. The discussion on f follows Ref. [41].

A.1 $\nu_s \rightarrow 3\nu$

The decay rate for this channel is

$$\Gamma_{3\nu} = \frac{G_F^2}{192\pi^3} m_s^5 \sin^2 \theta, \quad (\text{A.1})$$

where G_F is the Fermi constant, m_s is the mass of the sterile neutrino, and θ is the mixing angle between ν_e and ν_s . The neutrinos in the final state are decoupled from the thermal bath, then $f = 0$.

A.2 $\nu_s \rightarrow \nu_e + e^+ + e^-$

The decay rate for this channel is

$$\begin{aligned} \Gamma_{\nu_e^- e^+} &= \frac{G_F^2}{192\pi^3} m_s^5 \sin^2 \theta \\ &\times \left[\frac{1 + 4 \sin^2 \theta_w + 8 \sin^4 \theta_w}{4} \left((1 - 14x_e^2 - 2x_e^4 - 12x_e^6) \sqrt{1 - 4x_e^4} + 12x_e^4(x_e^4 - 1)L_e \right) \right. \\ &\quad \left. + 2 \sin^2 \theta_w (2 \sin^2 \theta_w + 1) \left(x_e^2(2 + 10x_e^2 - 12x_e^4) \sqrt{1 - 4x_e^4} + 6x_e^4(1 - 2x_e^2 + 2x_e^4)L_e \right) \right], \end{aligned} \quad (\text{A.2})$$

where

$$x_i \equiv \frac{m_i}{m_s}, \quad L_i \equiv \log \left[\frac{1 - 3x_i^2 - (1 - x_i^2) \sqrt{1 - 4x_i^2}}{x_i^2(1 + \sqrt{1 - 4x_i^2})} \right], \quad (i = e, \mu) \quad (\text{A.3})$$

and θ_w is the Weinberg angle. In this channel, the sterile neutrino mass is equally distributed to the three final state particles, which leads to $f \sim 2/3$

A.3 $\nu_s \rightarrow \nu_e + \mu^- + \mu^+$

The decay rate for this channel is

$$\begin{aligned} \Gamma_{\nu_e \mu^- \mu^+} &= \frac{G_F^2}{192\pi^3} m_s^5 \sin^2 \theta \\ &\times \left[\frac{1 - 4 \sin^2 \theta_w + 8 \sin^4 \theta_w}{4} \left((1 - 14x_\mu^2 - 2x_\mu^4 - 12x_\mu^6) \sqrt{1 - 4x_\mu^4} + 12x_\mu^4(x_\mu^4 - 1)L_\mu \right) \right. \\ &\quad \left. + 2 \sin^2 \theta_w (2 \sin^2 \theta_w - 1) \left(x_\mu^2(2 + 10x_\mu^2 - 12x_\mu^4) \sqrt{1 - 4x_\mu^4} + 6x_\mu^4(1 - 2x_\mu^2 + 2x_\mu^4)L_\mu \right) \right]. \end{aligned} \quad (\text{A.4})$$

This channel is available if $m_s \gtrsim 2m_\mu$. The produced muons decay mainly with $\mu^- \rightarrow e^- + \nu_\mu + \bar{\nu}_e$. In this process, each (anti-)neutrino has average energy $E_{\nu\mu} = 34.33$ MeV. Therefore, $f \sim 2/3 - 4E_{\nu\mu}/m_s$ when $m_s \gg 2m_\mu$.

A.4 $\nu_s \rightarrow e^- + \nu_\mu + \mu^+$

The decay rate for this channel is

$$\Gamma_{\nu_e \mu^- \mu^+} = \frac{G_F^2}{192\pi^3} m_s^5 \sin^2 \theta (1 - 8x_\mu^2 + 8x_\mu^6 - x_\mu^8 - 12x_\mu^4 \log x_\mu^2) \quad (\text{A.5})$$

This channel is available if $m_s \gtrsim m_e + m_\mu$. Like Sec. A.3, the muon decay take some energy away from the plasma and $f \sim 2/3 - 2E_{\nu\mu}/m_s$ when $m_s \gg m_e + m_\mu$.

A.5 $\nu_s \rightarrow \nu_e + \pi^0$

The decay rate for this channel is

$$\Gamma_{\nu_e \pi^0} = \frac{G_F^2 f_\pi^2}{32\pi} m_s^3 \left(1 - \frac{m_{\pi^0}^2}{m_s^2} \right)^2, \quad (\text{A.6})$$

where m_{π^0} is the neutral pion mass and $f_\pi = 130.2$ MeV is the pion decay constant. This channel is available if $m_s \gtrsim m_{\pi^0}$. The kinetic energy that the produced neutrino takes away is $(m_s^2 - m_{\pi^0}^2)/2m_s$ and $f \sim 1/2 + m_{\pi^0}^2/2m_s^2$.

A.6 $\nu_s \rightarrow e^- + \pi^+$

The decay rate for this channel is

$$\Gamma_{e^-\pi^+} = \frac{G_F^2 f_\pi^2}{16\pi} |V_{ud}| m_s^3 \sin^2 \theta \left(\left(1 - \frac{m_e^2}{m_s^2}\right)^2 - \frac{m_{\pi^+}^2}{m_s^2} \left(1 + \frac{m_e^2}{m_s^2}\right) \right) \times \sqrt{\left(1 - \frac{(m_{\pi^+} - m_e)^2}{m_s^2}\right) \left(1 - \frac{(m_{\pi^+} + m_e)^2}{m_s^2}\right)}, \quad (\text{A.7})$$

where V_{ud} is the CKM matrix element. This channel is available if $m_s \gtrsim m_{\pi^0}$. The produced charged pion decays mainly with $\pi^+ \rightarrow \mu^+ + \nu_\mu$ and the ν_μ has average energy $E_{\nu\pi} = 29.79$ MeV. The timescale of this decay is much shorter than the scattering and dynamical timescale, thus we can consider that this decay occurs instantaneously. The produced muon then decays into e^- , ν_μ , and $\bar{\nu}_e$. As a result, the average energy taken away to the decoupled neutrino sea is $\langle E_{\text{dec}} \rangle = E_{\nu\pi} + 2E_{\nu\mu} + (5/6)E_{\pi\text{KE}}$, where the kinetic energy of the pion is $E_{\pi\text{KE}} = m_s - E_e - m_{\pi^+}$ and the electron energy is $E_e = (m_s^2 - m_{\pi^+}^2 + m_e^2)/2m_s$. Therefore, $f \sim 1 - (E_{\nu\pi} + 2E_{\nu\mu} + (5/6)E_{\pi\text{KE}})/m_s$.

A.7 $\nu_s \rightarrow \nu_e + \gamma$

The decay rate for this channel is

$$\Gamma_{\nu\gamma} = \frac{9G_F^2}{512\pi^4} \alpha m_s^5 \sin^2 \theta, \quad (\text{A.8})$$

where α is the fine structure constant. Because ν_s is much heavier than ν_e and γ , the rest mass of the sterile neutrino is equally distributed into the two particles. Therefore, $f \sim 1/2$.

B Annihilation of high-energy neutrinos from the decay

Here we consider the correction to \bar{f} due to the scatterings and annihilations of the high energy active neutrinos produced from the sterile neutrino decays. While scatterings and annihilations have cross sections of similar magnitude, annihilation processes such as $\nu_e + \bar{\nu}_e \rightarrow e^- + e^+$ inject the maximal energy into the plasma. Therefore we focus on annihilation processes in order to evaluate the correction to \bar{f} . In addition, the decay process most relevant to the correction to \bar{f} is expected to emit high energy neutrino(s) and have a measurable branching ratio. From this point of view, we focus on the $\nu_s \rightarrow \nu_e + \pi^0$ channel.

B.1 Lorentz transformation of cross sections

First, we discuss the cross section. Let us consider the two massless particle that form the angle α . The momenta of these particle can be written as

$$p_A^\mu = E_A \begin{pmatrix} 1 \\ \sin \alpha/2 \\ \cos \alpha/2 \\ 0 \end{pmatrix}, \quad p_B^\mu = E_B \begin{pmatrix} 1 \\ -\sin \alpha/2 \\ \cos \alpha/2 \\ 0 \end{pmatrix}. \quad (\text{B.1})$$

By the Lorentz boost along the y axis, these momenta can be transformed to

$$p_{A'}^\mu = E_A \sin \alpha/2 \begin{pmatrix} 1 \\ 1 \\ 0 \\ 0 \end{pmatrix}, \quad p_{B'}^\mu = E_B \sin \alpha/2 \begin{pmatrix} 1 \\ -1 \\ 0 \\ 0 \end{pmatrix} \quad (\text{B.2})$$

and by making the Lorentz boost along the x axis successively, we obtain the momenta in the center of mass frame,

$$p_{A''}^\mu = \sqrt{E_A E_B} \sin \alpha/2 \begin{pmatrix} 1 \\ 1 \\ 0 \\ 0 \end{pmatrix}, \quad p_{B''}^\mu = \sqrt{E_A E_B} \sin \alpha/2 \begin{pmatrix} 1 \\ -1 \\ 0 \\ 0 \end{pmatrix}. \quad (\text{B.3})$$

Since the cross sections of two-body scatterings are given by

$$d\sigma = \frac{1}{2E_A 2E_B |v_A - v_B|} \left(\prod_f \frac{d^3 p_f}{(2\pi)^3} \right) \frac{1}{2E_f} |\mathcal{M}|^2 (2\pi)^4 \delta^{(4)}(p_A + p_B - \sum p_f), \quad (\text{B.4})$$

the dependence of the cross sections on frames is represented by $L \equiv 1/(E_A E_B |v_A - v_B|)$. $L = (2E_A E_B \sin \alpha/2)^{-1}$ in the first frame and $L'' = (E_A E_B \sin^2 \alpha/2)^{-1}$ in the center of mass frame. Therefore, we can obtain the relation between the cross section in the first frame σ and that in the center of mass frame σ_{CM} as

$$\sigma = \frac{L}{L''} \sigma_{\text{CM}} = \sigma_{\text{CM}} \sin \frac{\alpha}{2}. \quad (\text{B.5})$$

B.2 Annihilation of the decay products with the background neutrinos

Next we consider the annihilation of the decay products with the background neutrinos. In the following, we calculate the averaged probability $P_{\text{ann,BG}}$ that the neutrinos from the sterile neutrino decays annihilate with the background neutrinos. In the following we consider the cross sections in the center of mass frame of each process and then move to the rest frame of the radiation bath.

The amplitude squared $|\mathcal{M}|^2$ of $\nu_e(p_1) + \bar{\nu}_e(p_2) \rightarrow e^-(p_3) + e^+(p_4)$ is

$$|\mathcal{M}|^2 = 32G_F^2 [(C_V - C_A)^2 (p_1 \cdot p_3)^2 + (C_V + C_A)^2 (p_1 \cdot p_4)^2 + (C_V^2 - C_A^2) m_e^2 p_1 \cdot p_2], \quad (\text{B.6})$$

where $C_V = -0.5 + 2 \sin^2 \theta_W$, $C_A = -0.5$, and θ_W is the Weinberg angle. In our cases, since the momenta in the center of mass frame are much larger than m_e , we ignore the term with m_e^2 . By defining the angle made by \vec{p}_1 and \vec{p}_3 as θ , $|\mathcal{M}|^2$ can be rewritten as

$$|\mathcal{M}|^2 = 32G_F^2 E_1^4 [(C_V - C_A)^2 (1 - \cos \theta)^2 + (C_V + C_A)^2 (1 + \cos \theta)^2], \quad (\text{B.7})$$

where E_1 is the zero component of p_1^μ . In the center of mass frame, the cross section of $2 \rightarrow 2$ process is given by

$$\left(\frac{d\sigma}{d\Omega}\right)_{\text{CM}} = \frac{|\mathcal{M}|^2}{64\pi^2 (2E_1)^2} = \frac{G_F^2 E_1^2}{8\pi^2} [(C_V - C_A)^2 (1 - \cos \theta)^2 + (C_V + C_A)^2 (1 + \cos \theta)^2], \quad (\text{B.8})$$

where Ω is the solid angle of the final electron. By integrating over Ω , the total cross section is obtained as

$$\sigma_{\text{CM}} = \frac{4G_F^2 E_1^2}{3\pi} (C_V^2 + C_A^2). \quad (\text{B.9})$$

In the rest frame of the bath, we define the energy of the active neutrino produced in the sterile neutrino decay and the background neutrino as E_A and E_B . Then E_1 can be written in terms of E_A and E_B as

$$E_1 = \sqrt{E_A E_B} \sin \frac{\alpha}{2}, \quad (\text{B.10})$$

and the cross section in the rest frame is

$$\sigma = \frac{4G_F^2 E_A E_B}{3\pi} (C_V^2 + C_A^2) \sin^3 \frac{\alpha}{2} \quad (\text{B.11})$$

from (B.5). The cross section averaged over α can be obtained by integrating over $\cos \alpha$ as

$$\langle \sigma \rangle_\alpha = \frac{4G_F^2 E_A E_B}{3\pi} (C_V^2 + C_A^2) \int_{-1}^1 \frac{d \cos \alpha}{2} \sin^3 \frac{\alpha}{2} = \frac{8G_F^2 E_A E_B}{15\pi} (C_V^2 + C_A^2). \quad (\text{B.12})$$

Let us consider a sterile neutrino that decays at the time t_d and emits a neutrino with an energy E_ν and calculate the probability $\tilde{P}_{\text{ann,BG}}(t_d)$ that this neutrino annihilates with a background neutrino. Since the annihilation rate $\Gamma_{\text{ann,BG}} = \langle \sigma \rangle n_{\nu,\text{BG}}$ is proportional to the energies of neutrinos and the number density of background neutrinos, we can normalize the annihilation rate by using that just after the sterile neutrino decay at t_1 , $\Gamma_{\text{ann,BG}}(t_1)$ is

$$\Gamma_{\text{ann,BG}}(t) = \left(\frac{a(t)}{a(t_d)}\right)^{-1} \left(\frac{a(t)}{a(t_1)}\right)^{-4} \Gamma_{\text{ann,BG}}(t_1), \quad (\text{B.13})$$

where the first ratio of scale factors indicates the redshift of the neutrino produced in the decay and the second ratio of scale factors indicates the redshift of the background neutrinos. Here we take t_1 as the time when $\Gamma_{\text{decay}} = H(t_1)$. Therefore,

$$\begin{aligned} \tilde{P}_{\text{ann,BG}}(t_d) &= 1 - \exp \left[- \int_{t_d}^{\infty} dt \Gamma_{\text{ann,BG}}(t) \right] \\ &= 1 - \exp \left[- \int_{t_d}^{\infty} dt \left(\frac{a(t)}{a(t_d)}\right)^{-1} \left(\frac{a(t)}{a(t_1)}\right)^{-4} \Gamma_{\text{ann,BG}}(t_1) \right]. \end{aligned} \quad (\text{B.14})$$

In order to obtain the averaged probability $P_{\text{ann,BG}}$ that the neutrinos produced in the sterile neutrino decays annihilate with the background neutrinos, we convolute $\tilde{P}_{\text{ann,BG}}(t_d)$ with the time distribution of the sterile neutrino decays $\Gamma_{\text{decay}} \exp(-\Gamma_{\text{decay}} t_d)$:

$$\begin{aligned} P_{\text{ann,BG}} &= \int_0^\infty dt_d \Gamma_{\text{decay}} e^{-\Gamma_{\text{decay}} t_d} \tilde{P}_{\text{ann,BG}}(t_d) \\ &= \int_0^\infty dt_d \Gamma_{\text{decay}} e^{-\Gamma_{\text{decay}} t_d} \left(1 - \exp \left[- \int_{t_d}^\infty dt \left(\frac{a(t)}{a(t_d)} \right)^{-1} \left(\frac{a(t)}{a(t_1)} \right)^{-4} \Gamma_{\text{ann,BG}}(t_1) \right] \right). \end{aligned} \quad (\text{B.15})$$

For numerical evaluations, we assume the scale factor is proportional to a power of t : $a \propto t^s$. Then $H(t) = s/t$ and $\Gamma_{\text{decay}} = s/t_1$ follow. By using these equations, we can rewrite $P_{\text{ann,BG}}$ as

$$\begin{aligned} P_{\text{ann,BG}} &= s \int_0^\infty dx_d e^{-s x_d} \left(1 - \exp \left[-s x_d \frac{\Gamma_{\text{ann,BG}}(t_1)}{\Gamma_{\text{decay}}} \int_{x_d}^\infty dx x^{-5s} \right] \right) \\ &= s \int_0^\infty dx_d e^{-s x_d} \left(1 - \exp \left[-s \frac{x_d^{-4s+1}}{5s-1} \frac{\Gamma_{\text{ann,BG}}(t_1)}{\Gamma_{\text{decay}}} \right] \right) \end{aligned} \quad (\text{B.16})$$

Finally, let us calculate $\Gamma_{\text{ann,BG}}(t_1)$. At the time t_1 , the number density of the background neutrinos is

$$n_\nu(t_1) = \frac{3\zeta(3)}{4\pi^2} T_\nu^3(t_1) \quad (\text{B.17})$$

and the cross section is

$$\langle \sigma \rangle = \frac{8G_F^2 E_\nu \cdot 3.15 T_\nu(t_1)}{15\pi} (C_V^2 + C_A^2), \quad (\text{B.18})$$

where $3.15 T_\nu(t_1)$ is the thermal averaged energy of the background neutrino. Therefore

$$\Gamma_{\text{ann,BG}}(t_1) = \frac{2 \cdot 3.15 \zeta(3) G_F^2 E_\nu}{5\pi^3} \left(\frac{4}{11} \right)^{4/3} (C_V^2 + C_A^2) T_\gamma^4(t_1) \quad (\text{B.19})$$

where we used $T_\nu = (4/11)^{1/3} T_\gamma$. $T_\gamma(t_1)$ can be obtained from the Friedmann equation and the condition $H(t_1) = \Gamma_{\text{decay}}$:

$$H(t_1) = \sqrt{\frac{\rho_{\nu_s} + \rho_R}{3M_{\text{Pl}}^2}} = \frac{1}{\sqrt{3}M_{\text{Pl}}} \left[m_s n_{\nu_s}(T_\gamma(t_1)) + g_* \frac{\pi^2}{30} T_\gamma^4(t_1) \right]^{\frac{1}{2}} = \Gamma_{\text{decay}} \quad (\text{B.20})$$

By using (B.16), (B.19), and (B.20) and focusing on $\nu_e + \pi^0$ channel, we can calculate $P_{\text{ann,BG}}$ and the contribution of this process to the correction to \bar{f} , $\Delta \bar{f}_{\text{ann,BG},\nu_e\pi^0}$ from

$$\Delta \bar{f}_{\text{ann,BG},\nu_e\pi^0} = \left(\frac{1}{2} - \frac{m_{\pi^0}^2}{2m_s^2} \right) P_{\text{ann,BG}} B_{\nu_e\pi^0}, \quad (\text{B.21})$$

where $B_{\nu_e\pi^0} \equiv \Gamma_{\nu_e\pi^0}/\Gamma_{\text{decay}}$ is the branching ratio of $\nu_s \rightarrow \nu_e + \pi^0$.

B.3 Annihilation of the decay products with themselves

Annihilations of the decay products can be treated in a similar way. First we derive the probability $\tilde{P}_{\text{ann,D}}(t_d)$ that the neutrino produced at t_d annihilates. In this case, we have to integrate over the time \tilde{t} when the other annihilating neutrino is produced. Then we can represent the annihilation rate at t as

$$\Gamma_{\text{ann,D}}(t) = \tilde{\Gamma}_{\text{ann,D}}(t_1) \left(\frac{a(t)}{a(t_d)} \right)^{-1} \left(\frac{a(t)}{a(t_1)} \right)^{-3} \int_0^t d\tilde{t} \Gamma_{\text{decay}} e^{-\Gamma_{\text{decay}} \tilde{t}} \left(\frac{a(t)}{a(\tilde{t})} \right)^{-1}, \quad (\text{B.22})$$

where $\tilde{\Gamma}_{\text{ann,D}}(t_1)$ is the annihilation rate at t_1 for the neutrino produced at t_1 when we assume that all the sterile neutrinos instantaneously decay at t_1 . From a similar discussion, we obtain the averaged probability that the active neutrinos produced in the sterile neutrino decays annihilate with each other $P_{\text{ann,D}}$ as

$$P_{\text{ann,D}} = \int_0^\infty dt_d \Gamma_{\text{decay}} e^{-\gamma_{\text{decay}} t_d} \left(1 - \exp \left[- \int_{t_d}^\infty dt \Gamma_{\text{ann,D}}(t) \right] \right). \quad (\text{B.23})$$

In this case, because $\int_{t_d}^\infty dt \Gamma_{\text{ann,D}}(t)$ is always much smaller than unity, this equation can be approximated as

$$P_{\text{ann,D}} = \int_0^\infty dt_d \Gamma_{\text{decay}} e^{-\gamma_{\text{decay}} t_d} \int_{t_d}^\infty dt \Gamma_{\text{ann,D}}(t). \quad (\text{B.24})$$

By assuming $a \propto t^s$, this can be rewritten as

$$P_{\text{ann,D}} = s^3 \frac{\tilde{\Gamma}_{\text{ann,D}}(t_1)}{\Gamma_{\text{decay}}} \int_0^\infty dx_d e^{-s x_d} x_d^s \int_{x_d}^\infty dx x^{-5s} \int_0^x d\tilde{x} e^{-s\tilde{x}} \tilde{x}^s. \quad (\text{B.25})$$

Next we calculate $\tilde{\Gamma}_{\text{ann,D}}(t_1)$. Assuming an instantaneous decay and that the number density of the high energy neutrinos from the $\nu_e + \pi^0$ channel is $B_{\nu_e \pi^0} n_{\nu_s}(t_1)/2$, where the factor 1/2 comes from the distinction of neutrinos and anti-neutrinos. The cross section is

$$\langle \sigma \rangle = \frac{8G_F^2 E_\nu^2}{15\pi} (C_V^2 + C_A^2). \quad (\text{B.26})$$

Therefore

$$\tilde{\Gamma}_{\text{ann,D}}(t_1) = \frac{4G_F^2 E_\nu^2}{15\pi} B_{\nu_e \pi^0} (C_V^2 + C_A^2) n_{\nu_s}(t_1), \quad (\text{B.27})$$

where we used (B.20).

By using (B.25) and (B.27) and focusing on the $\nu_e + \pi^0$ channel, we can calculate $P_{\text{ann,D}}$ and the contribution of this process to the correction to \bar{f} , $\Delta \bar{f}_{\text{ann,D},\nu_e \pi^0}$,

$$\Delta \bar{f}_{\text{ann,D},\nu_e \pi^0} = \left(\frac{1}{2} - \frac{m_{\pi^0}^2}{2m_s^2} \right) P_{\text{ann,D}} B_{\nu_e \pi^0}. \quad (\text{B.28})$$

In Fig 5, we used $s = 2/3$, which gives larger corrections to \bar{f} than $s = 1/2$. We can check the contribution to the corrections to \bar{f} from the other decay processes are less than $\Delta \bar{f}_{\text{ann},\nu_e \pi^0}$ by similar calculations. In this work, we assume that the correction to \bar{f} can be regarded negligible in the region satisfying $\Delta \bar{f}_{\text{ann},\nu_e \pi^0} < 0.01$.

C BBN results in more detail

Here we show the results of the numerical BBN calculation with lepton asymmetries in more detail and make some comments on the choice of the observational constraints. In Fig. 13 and 14, we can find the regions that are consistent with the BBN constraints for $0.05 \lesssim \xi \lesssim 0.2$.

In Sec. 4 and 5, we adopt Cooke *et al.* [55] for D/H and Aver, Olive and Skillman [58] for Y_p . However we can consider several choices for the observational constraints. In Fig. 15, we compare the results when we adopt different observational constraints. As can be seen from Fig. 15, the existence of the consistent regions does not change. However the constraints are more severe when we adopt Izotov *et al.* [57] for the Y_P limits.

D Generation of a large lepton asymmetry

In this section we present a model for generating a large lepton asymmetry. The model is based on the Affleck-Dine mechanism in the minimal supersymmetric standard model (MSSM) [78, 79]. In the MSSM there exist many flat directions in the scalar potential of squark, slepton and Higgs fields [80]. Some flat directions have large field values during inflation. Such flat directions start to oscillate after inflation and produce a baryon (lepton) asymmetry if they have a baryon (lepton) number. This is called Affleck-Dine mechanism for baryogenesis or leptogenesis (for a review, see Ref. [81]). Here we focus on the Affleck-Dine leptogenesis in gauge-mediated SUSY breaking.

Suppose some flat direction (called AD field ϕ) with lepton number has a large field value during inflation. The potential of the AD field for $|\phi| \gg M_s$ is written as

$$\begin{aligned} V(\phi) &= V_{\text{gauge}} + V_{\text{grav}} + V_A \\ &= M_F^4 \left[\log \left(\frac{|\phi|^2}{M_s^2} \right) \right]^2 + m_{3/2}^2 |\phi|^2 \left(1 + K \log \frac{|\phi|^2}{M^2} \right) + V_A, \end{aligned} \quad (\text{D.1})$$

where M_s is the messenger scale, M_F is the SUSY breaking scale, $m_{3/2}$ is the gravitino mass, K is the coefficient of the one-loop correction and M is the renormalization scale. Here V_A is the A-term which generates the lepton asymmetry. V_{gauge} denotes the potential coming from the gauge-mediated SUSY breaking [82] and V_{grav} is due to the gravity mediation. The potential is dominated by V_{grav} for $|\phi| \gtrsim \varphi_{\text{eq}} \simeq M_F^2/m_{3/2}$. We assume that the field value $\varphi = |\phi|$ during inflation is much larger than φ_{eq} . When the Hubble parameter H becomes equal to the effective mass, i.e. $H \simeq m_{3/2}$, the AD field starts to oscillate. At the same time the AD field is kicked to the phase direction due to the A-term V_A , which leads to the generation of a lepton asymmetry. The produced lepton asymmetry is given by

$$\eta_L = \frac{n_L}{s} \simeq \varepsilon \frac{m_{3/2} \varphi_{\text{osc}}^2}{4m_{3/2}^2 M_p^2 / T_R} = \varepsilon \frac{T_R}{4m_{3/2}} \left(\frac{\varphi_{\text{osc}}}{M_p} \right)^2, \quad (\text{D.2})$$

where $\varphi_{\text{osc}} > \varphi_{\text{eq}}$ is the field value at the start of oscillation, T_R is the reheating temperature after inflation and $\varepsilon (\leq 1)$ is the parameter which represents the efficiency of the A-term.

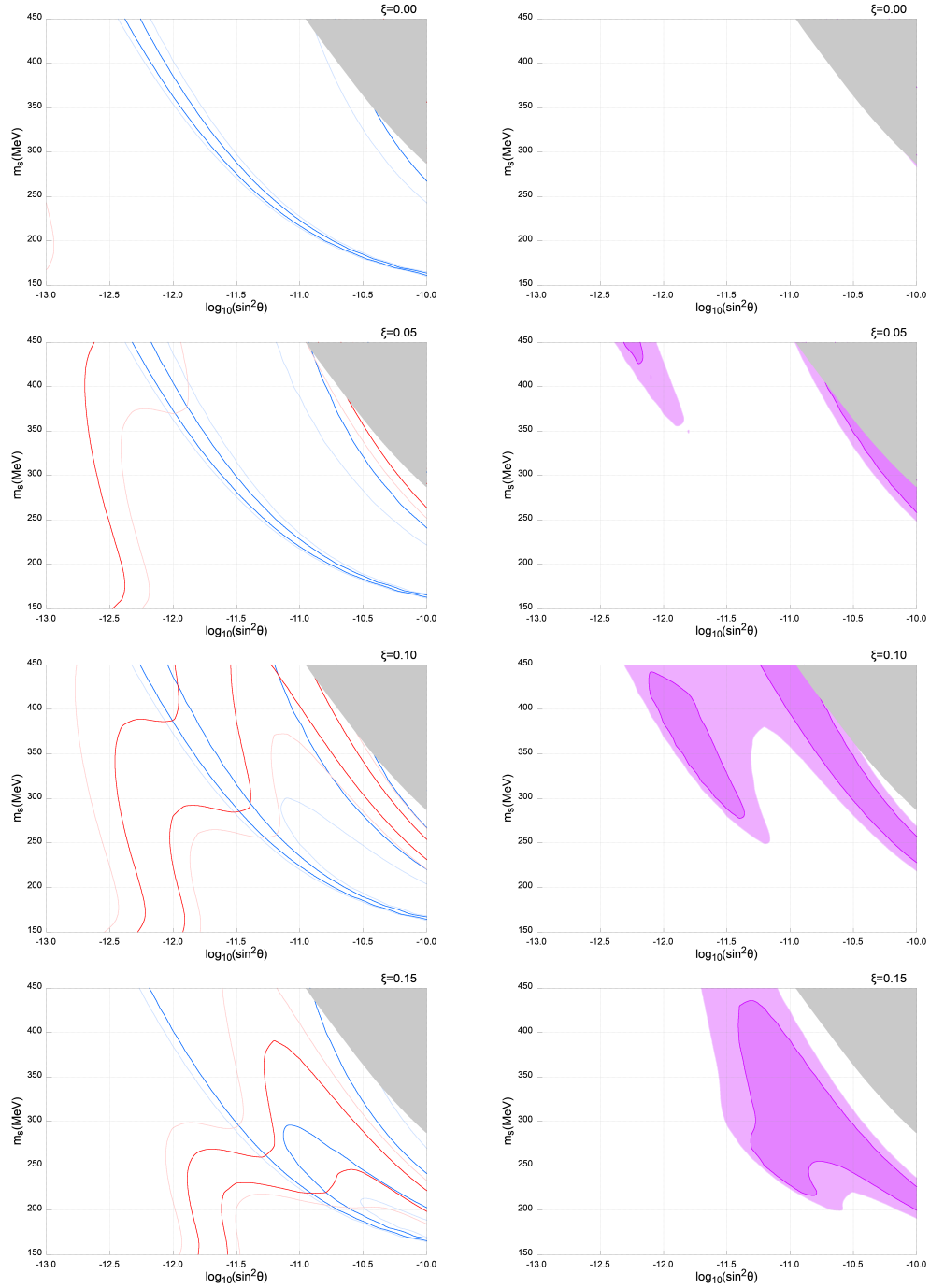


Figure 13: The result of the numerical calculation of BBN with the sterile neutrinos and lepton asymmetries from $\xi = 0, 0.05, 0.1$ and 0.15 .

Here we assumed that the oscillation starts before reheating and used the relation between the entropy s and total radiation densities ρ_R given by $s = 4\rho_R/3T$. Thus, the AD mechanism can generate a large lepton asymmetry. In the following we take $\varepsilon = 1$.

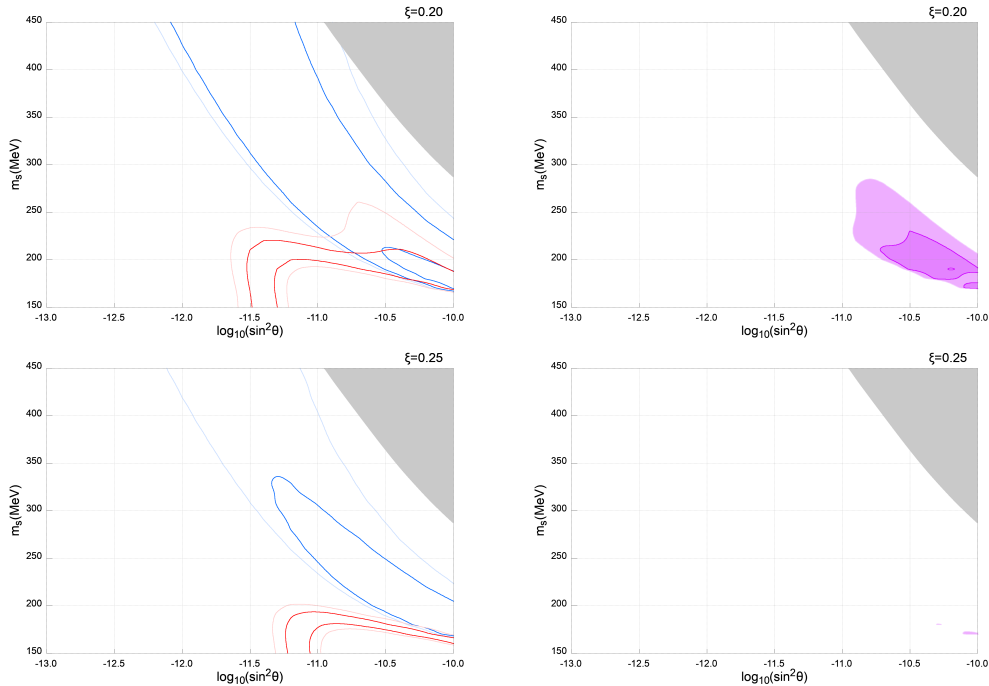


Figure 14: Same as Fig. 13 except for $\xi = 0.2$ and 0.25 .

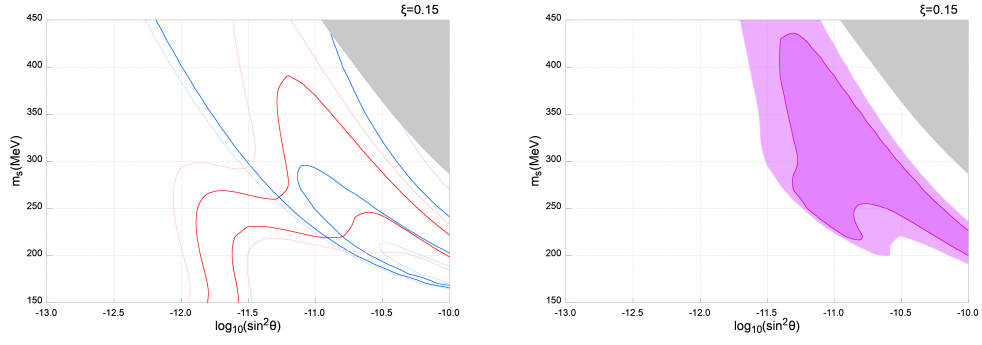
Another important consequence of the AD mechanism is the formation of Q-balls [83–88]. During oscillation the AD field fragments into spherical lumps through spatial instabilities of the field and almost all lepton number is confined within Q-balls. When the potential is dominated by V_{grav} the Q-ball formation depends on whether K is positive or negative. Since the instability of the AD field develops only for $K < 0$, Q-balls are (not) formed for $K < 0$ ($K > 0$) [89]. On the other hand, when the potential is dominated by V_{gauge} , Q-balls are always produced. Therefore, for $K > 0$ the Q-ball formation takes place when the AD field decreases to φ_{eq} . The Q-ball in this case is called delayed [90]. In the following we show that the delayed Q-balls in the AD mechanism produce a large lepton asymmetry without significant entropy production.³

The Q-balls with large lepton number decay by emitting neutrinos with decay rate [92, 93],

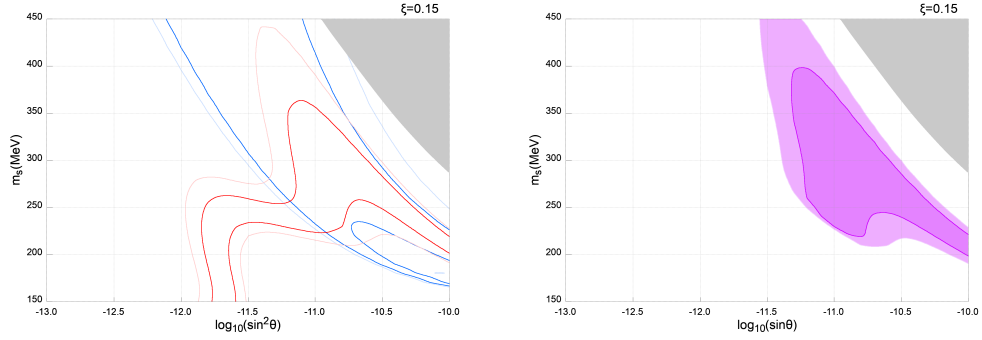
$$\Gamma_Q \simeq N_\ell \frac{1}{Q} \frac{\omega_Q^3}{12\pi^2} 4\pi R_Q^2, \quad (\text{D.3})$$

where Q is the Q-ball charge (= lepton number), ω_Q is the energy per charge, R_Q is the

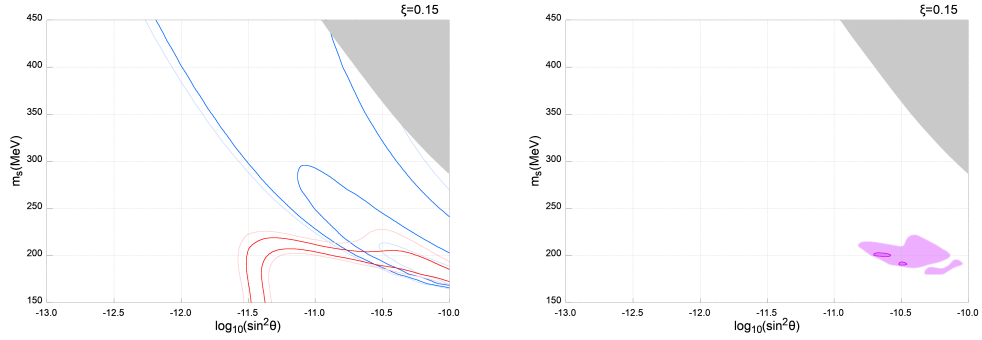
³Another scenario with large entropy production was proposed in Ref. [91].



(a) Cooke *et al.* [55] for D/H and Aver *et al.* [58] for Y_P



(b) Particle Data Group [53] for D/H and Y_P



(c) Cooke *et al.* [55] for D/H and Izotov *et al.* [57] for Y_P

Figure 15: The comparison of the BBN results with different observational estimates.

Q-ball radius and N_ℓ is the number of decay channels. ω_Q , R_Q and Q are given by [85, 86]

$$\omega_Q \simeq M_F Q^{-1/4}, \quad (\text{D.4})$$

$$R_Q \simeq M_F^{-1} Q^{1/4}, \quad (\text{D.5})$$

$$Q \simeq 6 \times 10^{-4} \left(\frac{\varphi_{\text{eq}}}{M_F} \right)^4. \quad (\text{D.6})$$

The cosmic temperature T_{QD} when the Q-balls decay is estimated as

$$\begin{aligned} T_{\text{QD}} &\simeq \left(\frac{90}{\pi^2 g_*(T_{\text{QD}})} \right)^{1/4} \sqrt{M_p \Gamma_Q} \\ &\simeq 0.018 \text{GeV} \left(\frac{g_*}{60.75} \right)^{-1/4} \left(\frac{N_\ell}{3} \right)^{1/2} \left(\frac{M_F}{10^5 \text{GeV}} \right)^{-2} \left(\frac{m_{3/2}}{0.1 \text{GeV}} \right)^{5/2}, \end{aligned} \quad (\text{D.7})$$

where g_* is the number of degrees of freedom at T_{QD} . The Q-ball energy density at T_{QD} is written as

$$\left. \frac{\rho_Q}{\rho_R} \right|_{T_{\text{QD}}} \simeq \frac{\omega_Q n_L}{(3/4) T_{\text{QD}} s(T_{\text{QD}})} \simeq 8.5 \frac{m_{3/2}}{T_{\text{QD}}} \eta_L. \quad (\text{D.8})$$

From Eq. (D.2) the lepton asymmetry η_L is written as

$$\eta_L \simeq 0.42 \left(\frac{T_R}{10^4 \text{GeV}} \right) \left(\frac{M_F}{10^5 \text{GeV}} \right)^4 \left(\frac{m_{3/2}}{0.1 \text{GeV}} \right)^{-3} \left(\frac{\varphi_{\text{osc}}}{10^5 \varphi_{\text{eq}}} \right)^2. \quad (\text{D.9})$$

For example, for $M_F = 0.9 \times 10^5$ GeV, $T_R = 1.5 \times 10^5$ GeV, $m_{3/2} = 0.6$ GeV and $\varphi_{\text{osc}} = 10^5 \varphi_{\text{eq}} \simeq 1.4 \times 10^{15}$ GeV, we obtain $\rho_Q/\rho_R \simeq 0.05$ and $\eta_L \simeq 0.02$. Therefore, a large lepton asymmetry is produced with negligible entropy production.

Lepton asymmetry is also produced from the Q-balls through evaporation [94, 95]. The evaporated charge ΔQ is written as [96]

$$\frac{\Delta Q}{Q} \sim 10^{-3} \left(\frac{M_s}{10^4 \text{GeV}} \right)^{-2/3} \left(\frac{M_F}{10^5 \text{GeV}} \right)^{-4} \left(\frac{m_{3/2}}{0.1 \text{GeV}} \right)^{11/3}, \quad (\text{D.10})$$

where M_s is the sparticle mass and the evaporation is most efficient around $T_*(< T_R)$ given by⁴

$$T_* \sim 10^3 \text{GeV} \left(\frac{M_s}{10^4 \text{GeV}} \right)^{2/3} \left(\frac{m_{3/2}}{0.1 \text{GeV}} \right)^{1/3}. \quad (\text{D.11})$$

(For $M_F = 0.9 \times 10^5$ GeV and $m_{3/2} = 0.6$ GeV, $\Delta Q/Q \sim 0.1$.) Thus, some fraction of the lepton charge of the Q-balls are emitted into the thermal plasma before the electroweak phase transition, which leads to a baryon asymmetry through the sphaleron effect. The produced baryon asymmetry η_B by the Q-ball evaporation is estimated as $\eta_B \sim (\Delta Q/Q) \eta_L$ which is too large for $\eta_L \sim 0.01$.

In order to avoid this problem, we need some mechanism to wash out the lepton asymmetry before the electroweak phase transition. This can be realized by introducing another sterile neutrino ν_h with a mass of $m_{hs} \sim 200$ GeV. Before the electroweak phase transition, sterile neutrinos interact with Higgs bosons and left-handed leptons through the Yukawa interaction and inverse decays of leptons and Higgs bosons into sterile neutrinos can wash out the lepton asymmetry contained in active neutrinos. The rate of washout $\Gamma_{\text{w.o.}}$ can be estimated as [97, 98]

$$\Gamma_{\text{w.o.}} \sim \frac{\lambda^2}{16\pi} m_{hs} \frac{K_1(m_{hs}/T)}{K_2(m_{hs}/T)} = \frac{m_{hs}^3}{16\pi v^2} \frac{K_1(m_{hs}/T)}{K_2(m_{hs}/T)} \sin^2 \theta_h, \quad (\text{D.12})$$

⁴The evaporated charge after the electroweak phase transition is suppressed by $(T_{\text{EW}}/T_*)^2$ compared with Eq. (D.10) where T_{EW} is the temperature at the electroweak phase transition.

where λ is the coupling constant of the Yukawa interaction, K_i is the modified Bessel function of order i , $v \simeq 246$ GeV is the vacuum expectation value of the Higgs field after the electroweak phase transition, and θ_h is the ν_h - ν_α mixing angle in the vacuum. In order to wash out the lepton asymmetry from the Q-ball evaporation, the washout process should be efficient just before the electroweak phase transition. Therefore, we require $\Gamma_{\text{w.o.}} \gg H$ at $T \sim 200$ GeV and derive the condition $\sin^2 \theta_h \gg 8 \times 10^{-14}$. In other words, if $m_h \sim 200$ GeV and $\sin^2 \theta_h \gg 8 \times 10^{-14}$, the lepton asymmetry from the Q-ball evaporation will be washed out to the extent consistent with the observed baryon asymmetry. This parameter region is free from observational or cosmological constraints [40, 99].

References

- [1] SUPER-KAMIOKANDE collaboration, Y. Fukuda et al., *Evidence for oscillation of atmospheric neutrinos*, *Phys. Rev. Lett.* **81** (1998) 1562 [[hep-ex/9807003](#)].
- [2] ALEPH, DELPHI, L3, OPAL, SLD, LEP ELECTROWEAK WORKING GROUP, SLD ELECTROWEAK GROUP, SLD HEAVY FLAVOUR GROUP collaboration, S. Schael et al., *Precision electroweak measurements on the Z resonance*, *Phys. Rept.* **427** (2006) 257 [[hep-ex/0509008](#)].
- [3] P. Minkowski, $\mu \rightarrow e\gamma$ at a Rate of One Out of 10^9 Muon Decays?, *Phys. Lett.* **67B** (1977) 421.
- [4] T. Yanagida, *Horizontal gauge symmetry and masses of neutrinos*, *Conf. Proc.* **C7902131** (1979) 95.
- [5] R. N. Mohapatra and G. Senjanovic, *Neutrino Mass and Spontaneous Parity Nonconservation*, *Phys. Rev. Lett.* **44** (1980) 912.
- [6] M. Gell-Mann, P. Ramond and R. Slansky, *Complex Spinors and Unified Theories*, *Conf. Proc.* **C790927** (1979) 315 [[1306.4669](#)].
- [7] MINIBOONE collaboration, A. A. Aguilar-Arevalo et al., *Significant Excess of ElectronLike Events in the MiniBooNE Short-Baseline Neutrino Experiment*, *Phys. Rev. Lett.* **121** (2018) 221801 [[1805.12028](#)].
- [8] LSND collaboration, A. Aguilar-Arevalo et al., *Evidence for neutrino oscillations from the observation of anti-neutrino(electron) appearance in a anti-neutrino(muon) beam*, *Phys. Rev.* **D64** (2001) 112007 [[hep-ex/0104049](#)].
- [9] C. Giunti and M. Laveder, *Statistical Significance of the Gallium Anomaly*, *Phys. Rev.* **C83** (2011) 065504 [[1006.3244](#)].
- [10] J. Kostensalo, J. Suhonen, C. Giunti and P. C. Srivastava, *The gallium anomaly revisited*, *Phys. Lett.* **B795** (2019) 542 [[1906.10980](#)].
- [11] G. Mention, M. Fechner, T. Lasserre, T. A. Mueller, D. Lhuillier, M. Cribier et al., *The Reactor Antineutrino Anomaly*, *Phys. Rev.* **D83** (2011) 073006 [[1101.2755](#)].
- [12] M. Dentler, Á. Hernández-Cabezudo, J. Kopp, P. A. N. Machado, M. Maltoni, I. Martinez-Soler et al., *Updated Global Analysis of Neutrino Oscillations in the Presence of eV-Scale Sterile Neutrinos*, *JHEP* **08** (2018) 010 [[1803.10661](#)].
- [13] S. Gariazzo, C. Giunti, M. Laveder and Y. F. Li, *Model-independent $\bar{\nu}_e$ short-baseline oscillations from reactor spectral ratios*, *Phys. Lett.* **B782** (2018) 13 [[1801.06467](#)].
- [14] J. Liao, D. Marfatia and K. Whisnant, *MiniBooNE, MINOS+ and IceCube data imply a baroque neutrino sector*, *Phys. Rev.* **D99** (2019) 015016 [[1810.01000](#)].

- [15] NEOS collaboration, Y. J. Ko et al., *Sterile Neutrino Search at the NEOS Experiment*, *Phys. Rev. Lett.* **118** (2017) 121802 [[1610.05134](#)].
- [16] DANSS collaboration, I. Alekseev et al., *Search for sterile neutrinos at the DANSS experiment*, *Phys. Lett.* **B787** (2018) 56 [[1804.04046](#)].
- [17] S. Dodelson and L. M. Widrow, *Sterile-neutrinos as dark matter*, *Phys. Rev. Lett.* **72** (1994) 17 [[hep-ph/9303287](#)].
- [18] X.-D. Shi and G. M. Fuller, *A New dark matter candidate: Nonthermal sterile neutrinos*, *Phys. Rev. Lett.* **82** (1999) 2832 [[astro-ph/9810076](#)].
- [19] A. D. Dolgov and S. H. Hansen, *Massive sterile neutrinos as warm dark matter*, *Astropart. Phys.* **16** (2002) 339 [[hep-ph/0009083](#)].
- [20] K. Abazajian, G. M. Fuller and M. Patel, *Sterile neutrino hot, warm, and cold dark matter*, *Phys. Rev.* **D64** (2001) 023501 [[astro-ph/0101524](#)].
- [21] K. Abazajian, G. M. Fuller and W. H. Tucker, *Direct detection of warm dark matter in the X-ray*, *Astrophys. J.* **562** (2001) 593 [[astro-ph/0106002](#)].
- [22] T. Asaka, S. Blanchet and M. Shaposhnikov, *The ν MSM, dark matter and neutrino masses*, *Phys. Lett.* **B631** (2005) 151 [[hep-ph/0503065](#)].
- [23] T. Asaka and M. Shaposhnikov, *The ν MSM, dark matter and baryon asymmetry of the universe*, *Phys. Lett.* **B620** (2005) 17 [[hep-ph/0505013](#)].
- [24] M. Shaposhnikov and I. Tkachev, *The ν MSM, inflation, and dark matter*, *Phys. Lett.* **B639** (2006) 414 [[hep-ph/0604236](#)].
- [25] A. Kusenko, *Sterile neutrinos, dark matter, and the pulsar velocities in models with a Higgs singlet*, *Phys. Rev. Lett.* **97** (2006) 241301 [[hep-ph/0609081](#)].
- [26] K. Petraki and A. Kusenko, *Dark-matter sterile neutrinos in models with a gauge singlet in the Higgs sector*, *Phys. Rev.* **D77** (2008) 065014 [[0711.4646](#)].
- [27] K. Petraki, *Small-scale structure formation properties of chilled sterile neutrinos as dark matter*, *Phys. Rev. D* **77** (2008) 105004 [[0801.3470](#)].
- [28] M. Loewenstein, A. Kusenko and P. L. Biermann, *New Limits on Sterile Neutrinos from Suzaku Observations of the Ursa Minor Dwarf Spheroidal Galaxy*, *Astrophys. J.* **700** (2009) 426 [[0812.2710](#)].
- [29] M. Loewenstein and A. Kusenko, *Dark Matter Search Using Chandra Observations of Willman 1, and a Spectral Feature Consistent with a Decay Line of a 5 keV Sterile Neutrino*, *Astrophys. J.* **714** (2010) 652 [[0912.0552](#)].
- [30] A. Kusenko, F. Takahashi and T. T. Yanagida, *Dark Matter from Split Seesaw*, *Phys. Lett. B* **693** (2010) 144 [[1006.1731](#)].
- [31] M. Loewenstein and A. Kusenko, *Dark Matter Search Using XMM-Newton Observations of Willman 1*, *Astrophys. J.* **751** (2012) 82 [[1203.5229](#)].
- [32] M. Drewes et al., *A White Paper on keV Sterile Neutrino Dark Matter*, *JCAP* **1701** (2017) 025 [[1602.04816](#)].
- [33] K. N. Abazajian and A. Kusenko, *Hidden treasures: Sterile neutrinos as dark matter with miraculous abundance, structure formation for different production mechanisms, and a solution to the σ_8 problem*, *Phys. Rev. D* **100** (2019) 103513 [[1907.11696](#)].
- [34] A. Kusenko and G. Segre, *Neutral current induced neutrino oscillations in a supernova*, *Phys. Lett. B* **396** (1997) 197 [[hep-ph/9701311](#)].
- [35] A. Kusenko and G. Segre, *Pulsar kicks from neutrino oscillations*, *Phys. Rev. D* **59** (1999) 061302 [[astro-ph/9811144](#)].

- [36] G. M. Fuller, A. Kusenko and K. Petraki, *Heavy sterile neutrinos and supernova explosions*, *Phys. Lett. B* **670** (2009) 281 [0806.4273].
- [37] M. Fukugita and T. Yanagida, *Baryogenesis Without Grand Unification*, *Phys. Lett.* **B174** (1986) 45.
- [38] M. A. Luty, *Baryogenesis via leptogenesis*, *Phys. Rev.* **D45** (1992) 455.
- [39] E. K. Akhmedov, V. A. Rubakov and A. Yu. Smirnov, *Baryogenesis via neutrino oscillations*, *Phys. Rev. Lett.* **81** (1998) 1359 [hep-ph/9803255].
- [40] A. Kusenko, *Sterile neutrinos: The Dark side of the light fermions*, *Phys. Rept.* **481** (2009) 1 [0906.2968].
- [41] G. M. Fuller, C. T. Kishimoto and A. Kusenko, *Heavy sterile neutrinos, entropy and relativistic energy production, and the relic neutrino background*, **1110.6479**.
- [42] S. H. Hansen and Z. Haiman, *Do we need stars to reionize the universe at high redshifts? Early reionization by decaying heavy sterile neutrinos*, *Astrophys. J.* **600** (2004) 26 [astro-ph/0305126].
- [43] A. Boyarsky, O. Ruchayskiy and M. Shaposhnikov, *The Role of sterile neutrinos in cosmology and astrophysics*, *Ann. Rev. Nucl. Part. Sci.* **59** (2009) 191 [0901.0011].
- [44] P. D. Bolton, F. F. Deppisch and P. S. B. Dev, *Neutrinoless double beta decay versus other probes of heavy sterile neutrinos*, **1912.03058**.
- [45] A. D. Dolgov, S. H. Hansen, G. Raffelt and D. V. Semikoz, *Cosmological and astrophysical bounds on a heavy sterile neutrino and the KARMEN anomaly*, *Nucl. Phys.* **B580** (2000) 331 [hep-ph/0002223].
- [46] A. D. Dolgov, S. H. Hansen, G. Raffelt and D. V. Semikoz, *Heavy sterile neutrinos: Bounds from big bang nucleosynthesis and SN1987A*, *Nucl. Phys.* **B590** (2000) 562 [hep-ph/0008138].
- [47] O. Ruchayskiy and A. Ivashko, *Restrictions on the lifetime of sterile neutrinos from primordial nucleosynthesis*, *JCAP* **1210** (2012) 014 [1202.2841].
- [48] A. C. Vincent, E. F. Martinez, P. Hernández, M. Lattanzi and O. Mena, *Revisiting cosmological bounds on sterile neutrinos*, *JCAP* **1504** (2015) 006 [1408.1956].
- [49] G. B. Gelmini, P. Lu and V. Takhistov, *Cosmological Dependence of Non-resonantly Produced Sterile Neutrinos*, *JCAP* **1912** (2019) 047 [1909.13328].
- [50] T. Rehagen and G. B. Gelmini, *Effects of kination and scalar-tensor cosmologies on sterile neutrinos*, *JCAP* **06** (2014) 044 [1402.0607].
- [51] G. B. Gelmini, P. Lu and V. Takhistov, *Cosmological Dependence of Resonantly Produced Sterile Neutrinos*, **1911.03398**.
- [52] R. H. Cyburt, B. D. Fields, K. A. Olive and T.-H. Yeh, *Big Bang Nucleosynthesis: 2015*, *Rev. Mod. Phys.* **88** (2016) 015004 [1505.01076].
- [53] PARTICLE DATA GROUP collaboration, M. Tanabashi et al., *Review of Particle Physics*, *Phys. Rev.* **D98** (2018) 030001.
- [54] D. Gorbunov and M. Shaposhnikov, *How to find neutral leptons of the ν MSM?*, *JHEP* **10** (2007) 015 [0705.1729].
- [55] R. J. Cooke, M. Pettini and C. C. Steidel, *One Percent Determination of the Primordial Deuterium Abundance*, *Astrophys. J.* **855** (2018) 102 [1710.11129].
- [56] E. O. Zavarygin, J. K. Webb, S. Riemer-Sørensen and V. Dumont, *Primordial deuterium abundance at $z_{abs} = 2:504$ towards Q1009+2956*, *J. Phys. Conf. Ser.* **1038** (2018) 012012 [1801.04704].

- [57] Y. I. Izotov, T. X. Thuan and N. G. Guseva, *A new determination of the primordial He abundance using the He I $\lambda 10830$ Å emission line: cosmological implications*, *Monthly Notices of the Royal Astronomical Society* **445** (2014) 778 [[1408.6953](#)].
- [58] E. Aver, K. A. Olive and E. D. Skillman, *The effects of He I $\lambda 10830$ on helium abundance determinations*, *JCAP* **1507** (2015) 011 [[1503.08146](#)].
- [59] V. Fernández, E. Terlevich, A. I. Díaz, R. Terlevich and F. F. Rosales-Ortega, *Primordial helium abundance determination using sulphur as metallicity tracer*, *Monthly Notices of the Royal Astronomical Society* **478** (2018) 5301–5319.
- [60] M. Valerdi, A. Peimbert, M. Peimbert and A. Sixtos, *Determination of the Primordial Helium Abundance Based on NGC 346, an H II Region of the Small Magellanic Cloud*, *Astrophys. J.* **876** (2019) 98 [[1904.01594](#)].
- [61] PLANCK collaboration, N. Aghanim et al., *Planck 2018 results. VI. Cosmological parameters*, [1807.06209](#).
- [62] O. Pisanti, A. Cirillo, S. Esposito, F. Iocco, G. Mangano, G. Miele et al., *PARthENoPE: Public Algorithm Evaluating the Nucleosynthesis of Primordial Elements*, *Comput. Phys. Commun.* **178** (2008) 956 [[0705.0290](#)].
- [63] R. Consiglio, P. F. de Salas, G. Mangano, G. Miele, S. Pastor and O. Pisanti, *PARthENoPE reloaded*, *Comput. Phys. Commun.* **233** (2018) 237 [[1712.04378](#)].
- [64] J. L. Bernal, L. Verde and A. G. Riess, *The trouble with H_0* , *JCAP* **1610** (2016) 019 [[1607.05617](#)].
- [65] L. A. Popa and A. Vasile, *WMAP 5-year constraints on lepton asymmetry and radiation energy density: Implications for Planck*, *JCAP* **0806** (2008) 028 [[0804.2971](#)].
- [66] A. Caramete and L. Popa, *Cosmological evidence for leptonic asymmetry after Planck*, *JCAP* **02** (2014) 012 [[1311.3856](#)].
- [67] R. C. Nunes and A. Bonilla, *Probing the properties of relic neutrinos using the cosmic microwave background, the Hubble Space Telescope and galaxy clusters*, *Mon. Not. Roy. Astron. Soc.* **473** (2018) 4404 [[1710.10264](#)].
- [68] T2K collaboration, K. Abe et al., *Search for heavy neutrinos with the T2K near detector ND280*, *Phys. Rev.* **D100** (2019) 052006 [[1902.07598](#)].
- [69] NA62 collaboration, E. Cortina Gil et al., *Search for heavy neutral lepton production in K^+ decays*, *Phys. Lett.* **B778** (2018) 137 [[1712.00297](#)].
- [70] G. Bernardi et al., *Search for Neutrino Decay*, *Phys. Lett.* **166B** (1986) 479.
- [71] G. Bernardi et al., *FURTHER LIMITS ON HEAVY NEUTRINO COUPLINGS*, *Phys. Lett.* **B203** (1988) 332.
- [72] P. Coloma, P. Hernández, V. Muñoz and I. M. Shoemaker, *New constraints on Heavy Neutral Leptons from Super-Kamiokande data*, *Eur. Phys. J.* **C80** (2020) 235 [[1911.09129](#)].
- [73] A. Kusenko, S. Pascoli and D. Semikoz, *New bounds on MeV sterile neutrinos based on the accelerator and Super-Kamiokande results*, *JHEP* **11** (2005) 028 [[hep-ph/0405198](#)].
- [74] NA62 collaboration, C. Lazzeroni et al., *Precision Measurement of the Ratio of the Charged Kaon Leptonic Decay Rates*, *Phys. Lett.* **B719** (2013) 326 [[1212.4012](#)].
- [75] D. A. Bryman and R. Shrock, *Constraints on Sterile Neutrinos in the MeV to GeV Mass Range*, *Phys. Rev.* **D100** (2019) 073011 [[1909.11198](#)].
- [76] E. Grohs, G. M. Fuller and M. Sen, *Consequences of neutrino self interactions for weak decoupling and big bang nucleosynthesis*, [2002.08557](#).

- [77] G. B. Gelmini, A. Kusenko and V. Takhistov, *Hints of Sterile Neutrinos in Recent Measurements of the Hubble Parameter*, [1906.10136](#).
- [78] I. Affleck and M. Dine, *A New Mechanism for Baryogenesis*, *Nucl. Phys.* **B249** (1985) 361.
- [79] M. Dine, L. Randall and S. D. Thomas, *Baryogenesis from flat directions of the supersymmetric standard model*, *Nucl. Phys.* **B458** (1996) 291 [[hep-ph/9507453](#)].
- [80] T. Gherghetta, C. F. Kolda and S. P. Martin, *Flat directions in the scalar potential of the supersymmetric standard model*, *Nucl. Phys. B* **468** (1996) 37 [[hep-ph/9510370](#)].
- [81] M. Dine and A. Kusenko, *The Origin of the matter - antimatter asymmetry*, *Rev. Mod. Phys.* **76** (2003) 1 [[hep-ph/0303065](#)].
- [82] A. de Gouvea, T. Moroi and H. Murayama, *Cosmology of supersymmetric models with low-energy gauge mediation*, *Phys. Rev. D* **56** (1997) 1281 [[hep-ph/9701244](#)].
- [83] S. R. Coleman, *Q Balls*, *Nucl. Phys. B* **262** (1985) 263.
- [84] A. Kusenko, *Solitons in the supersymmetric extensions of the standard model*, *Phys. Lett. B* **405** (1997) 108 [[hep-ph/9704273](#)].
- [85] G. Dvali, A. Kusenko and M. E. Shaposhnikov, *New physics in a nutshell, or Q ball as a power plant*, *Phys. Lett. B* **417** (1998) 99 [[hep-ph/9707423](#)].
- [86] A. Kusenko and M. E. Shaposhnikov, *Supersymmetric Q balls as dark matter*, *Phys. Lett. B* **418** (1998) 46 [[hep-ph/9709492](#)].
- [87] K. Enqvist and J. McDonald, *Q balls and baryogenesis in the MSSM*, *Phys. Lett. B* **425** (1998) 309 [[hep-ph/9711514](#)].
- [88] S. Kasuya and M. Kawasaki, *Q ball formation through Affleck-Dine mechanism*, *Phys. Rev. D* **61** (2000) 041301 [[hep-ph/9909509](#)].
- [89] S. Kasuya and M. Kawasaki, *A New type of stable Q balls in the gauge mediated SUSY breaking*, *Phys. Rev. Lett.* **85** (2000) 2677 [[hep-ph/0006128](#)].
- [90] S. Kasuya and M. Kawasaki, *Q ball formation: Obstacle to Affleck-Dine baryogenesis in the gauge mediated SUSY breaking?*, *Phys. Rev. D* **64** (2001) 123515 [[hep-ph/0106119](#)].
- [91] M. Kawasaki, F. Takahashi and M. Yamaguchi, *Large lepton asymmetry from Q balls*, *Phys. Rev. D* **66** (2002) 043516 [[hep-ph/0205101](#)].
- [92] A. G. Cohen, S. R. Coleman, H. Georgi and A. Manohar, *The Evaporation of Q Balls*, *Nucl. Phys. B* **272** (1986) 301.
- [93] M. Kawasaki and M. Yamada, *Q ball Decay Rates into Gravitinos and Quarks*, *Phys. Rev. D* **87** (2013) 023517 [[1209.5781](#)].
- [94] M. Laine and M. E. Shaposhnikov, *Thermodynamics of nontopological solitons*, *Nucl. Phys. B* **532** (1998) 376 [[hep-ph/9804237](#)].
- [95] R. Banerjee and K. Jedamzik, *On B-ball dark matter and baryogenesis*, *Phys. Lett. B* **484** (2000) 278 [[hep-ph/0005031](#)].
- [96] S. Kasuya and M. Kawasaki, *Baryogenesis from the gauge-mediation type Q-ball and the new type of Q-ball as the dark matter*, *Phys. Rev. D* **89** (2014) 103534 [[1402.4546](#)].
- [97] W. Buchmuller, P. Di Bari and M. Plumacher, *Leptogenesis for pedestrians*, *Annals Phys.* **315** (2005) 305 [[hep-ph/0401240](#)].
- [98] W. Buchmuller, R. Peccei and T. Yanagida, *Leptogenesis as the origin of matter*, *Ann. Rev. Nucl. Part. Sci.* **55** (2005) 311 [[hep-ph/0502169](#)].
- [99] M. Drewes and B. Garbrecht, *Combining experimental and cosmological constraints on heavy neutrinos*, *Nucl. Phys. B* **921** (2017) 250 [[1502.00477](#)].